VNiVERSiDAD D SALAMANCA

TRABAJO DE FIN DE GRADO

Astrophysical signatures of theories with screening mechanisms

Author
María Rodríguez Domínguez

Tutors
Jose Beltrán Jiménez
Dario Bettoni

Grado en física
Facultad de Ciencias

Salamanca, 2024

VNiVERSiDAD D SALAMANCA

TRABAJO DE FIN DE GRADO

Astrophysical signatures of theories with screening mechanisms

Author
María Rodríguez Domínguez

Tutors
Jose Beltrán Jiménez
Dario Bettoni

Grado en física
Facultad de Ciencias

Salamanca, 2024

Student's signature:

RODRIGUEZ DOMINGUEZ MARIA - 54430577L

Firmado digitalmente por RODRIGUEZ DOMINGUEZ MARIA - 54430577L
Fecha: 2024.07.02 16:42:28 +02'00'

D. Jose Beltrán Jiménez y **D. Dario Bettoni** hacen constar que el trabajo titulado ASTROPHYSICAL SIGNATURES OF THEORIES WITH SCREENING MECHANISMS, ha sido realizado por María Rodríguez Domínguez, con DNI ****0577L y constituye la memoria del trabajo realizado para la superación de la asignatura Trabajo de Fin de Grado en Física en esta universidad.

En Salamanca, a fecha de firma electrónica.

Firmado por BELTRAN JIMENEZ JOSE - ***5470** el día 02/07/2024 con un certificado emitido por AC FNMT Usuarios

Fdo.: JOSE BELTRÁN JIMÉNEZ

Firmado por BETTONI DARIO - ****7229* el día 02/07/2024 con un certificado emitido por AC FNMT Usuarios

Fdo.: DARIO BETTONI

and she falls into the light swaying and she feels nice and warm as she lies there, in this cold night, and she looks up at the clear stars and the round shining moon
Now life begins, she says
Now we're sailing into life, he says
and then she hears the sea coming, and the sea going, and the moon is shining and the night is like a strange day and the boat is drifting and drifting forward, southward, along the foreshore

TRILOGY, Jon Fosse

Abstract

The Standard Cosmological Model, ΛCDM, introduces a cosmological constant in order to explain the accelerated expansion of the universe. However, this solution presents theoretical problems, which, together with the possibility that this acceleration is produced by new fields, leads up to the formulation of theoretical alternatives. In particular, we will center our attention on scalar fields. These fields typically couple to matter in such a way that they lead to new forces. In order for these theories to match observational constraints in the Solar System, they must be equipped with screening mechanisms that hide the forces in high-density regions.

After reviewing these mechanisms, we will obtain analytical results for the cases of *symmetron* and *chameleon*, as well as presenting a numerical approach to compare the solutions. Then, we will go on to study theories with kinetic screening, and we will obtain the equation for the profile of the field for static and non-relativistic sources. Giving the non-linearities of this equation, we will present the irrotational approximation, which simplifies the theoretical calculations, and we will develop a code aimed at finding numerical solutions for the field in general situations.

We will center our efforts in the Dirac-Born-Infeld theory, and we will use this code to prove the existence of regions in which the screening breaks down when there is more than one mass. Lastly, we will compare the numerical results to those given by the irrotational approximation, thus checking its validity.

Keywords: Cosmology, Scalar Fields, Screening Mechanisms, Kinectic Screening, Dirac-Born-Infeld, Python

Resumen

El Modelo Cosmológico Estándar, ΛCDM, introduce una constante cosmológica para explicar la expansión acelerada del universo. Sin embargo, esto presenta problemas de naturalidad, los cuales, junto con la posibilidad de que esta expansión sea provocada por nuevos campos, llevan a la formulación de alternativas teóricas. En particular, nos centraremos en campos escalares. Estos campos deben acoplarse a la materia de tal manera que conduzcan a nuevas fuerzas. Para que estas teorías sean compatibles con las restricciones observacionales, deben estar equipadas con mecanismos de apantallamiento que escondan las fuerzas en regiones de alta densidad.

Después de revisar estos mecanismos, obtendremos resultados analíticos para los casos de *symmetron* y *chameleon*, así como presentaremos un enfoque numérico para comparar las soluciones. A continuación, estudiaremos teorías con apantallamiento cinético y obtendremos la ecuación para el perfil del campo para fuentes estáticas y no relativistas. Dada la no linealidad de esta ecuación, presentaremos la aproximación irrotacional, que simplifica los cálculos teóricos, y desarrollaremos un código destinado a encontrar soluciones numéricas para el campo en situaciones generales.

Finalmente, centraremos nuestros esfuerzos en la teoría de Dirac-Born-Infeld, y utilizaremos este código para demostrar la existencia de regiones en las que el apantallamiento se rompe en presencia de más de una masa. Por último, compararemos los resultados numéricos con los dados por la aproximación irrotacional, comprobando así su validez.

Palabras clave: Cosmología, Campos Escalares, Mecanismos de Apantallamiento, Apantallamiento Cinético, Dirac-Born-Infeld, Python

Contents

Chapter 1

Introduction

Einstein's General Relativity is the modern description for gravitation, and it relates the curvature of spacetime to its content of matter and energy. It can be derived from Einstein-Hilbert action

$$S = \frac{1}{16\pi G}\int d^4x\ \sqrt{-g}R + S_m, \tag{1.1}$$

where S_m is the action for matter fields, g is the determinant of the metric of spacetime and R the Ricci scalar. Imposing that $\delta_g S = 0$, we find the field equations

$$R_{\mu\nu} - \frac{1}{2}g_{\mu\nu}R = 8\pi G T_{\mu\nu}, \tag{1.2}$$

where $T_{\mu\nu}$ is the stress-energy tensor, given by

$$T_{\mu\nu} = \frac{2}{\sqrt{-g}}\frac{\delta(\sqrt{-g}\mathcal{L})}{\delta g^{\mu\nu}}. \tag{1.3}$$

These Greek indexes range from 0 to 3. We will from now on explore how we can apply these equations to the study of the behaviour of our universe: its shape, its contents and its evolution, as well as whether we can modify gravity to better explain observations.

1.1 The expanding universe

Cosmology bases its study of the universe in two basic ideas: the cosmological principle and Weyl's Postulate. The cosmological principle states that at any time, the universe is homogeneous and isotropic at large scales, which implies that all points and directions in space are equivalent. This propriety defines maximally symmetric spaces, which are characterised by having a constant curvature. In addition, Weyl's Postulate models the matter of the universe as a perfect fluid, whose components move along temporal geodesics. This defines a privileged system of reference in which observers are at rest with respect to the cosmic fluid, known as comoving observers.

1.1.1 The Friedmann equations

As a consequence of the cosmological principle, we will describe spacetime as a manifold that can be described as a collection of spatial three-dimensional maximally symmetryc hypersurfaces. Thus, we can work with the Friedmann-Lemaître-Robertson-Walker metric (FLRW):

$$ds^2 = -dt^2 + a(t)^2 \left(\frac{dr^2}{1-kr^2} + r^2(d\theta^2 + \sin^2\theta d\varphi^2) \right), \tag{1.4}$$

where k is a constant that can have the values +1, 0 or -1 and represents the global curvature of the spatial sections: $k = 0$ describes flat space, while $k = +1$ represents spherical geometry and $k = -1$ represents hyperbolic geometry. The dimensionless function $a(t)$ is known as cosmic scale factor.

For a perfect fluid, the stress-energy tensor is given in the comoving reference frame by

$$T_{\mu\nu} = \begin{pmatrix} \rho & 0 & 0 & 0 \\ 0 & P & 0 & 0 \\ 0 & 0 & P & 0 \\ 0 & 0 & 0 & P \end{pmatrix}. \tag{1.5}$$

Computing the curvature of the metric (1.4) and using the field equations, it is possible to find Friedmann's equations

$$\left(\frac{\dot{a}}{a}\right)^2 = \frac{8\pi G}{3}\rho - \frac{k}{a^2}, \tag{1.6}$$

$$\frac{\ddot{a}}{a} = -\frac{8\pi G}{6}\rho(1+3w), \tag{1.7}$$

which relate the evolution of the scale factor with the global geometry of the universe and its matter content. We have defined $w = \frac{P}{\rho}$. The density parameter of a certain species i can be defined as

$$\Omega_i = \frac{\rho_i}{\rho_c}, \tag{1.8}$$

where $\rho_c = \frac{3H^2}{8\pi G}$ is the critical density.

1.1.2 The accelerated expansion of the universe

The solutions to these equations predict a universe that evolves with time, something that did not match the generalized beliefs at the beginning of the 20th century. For this reason, Einstein added another term to his equations that allowed for a static solution, known as the cosmological constant, Λ. Thus, the equations become

$$R_{\mu\nu} - \frac{1}{2}g_{\mu\nu}R - 8\pi G\Lambda g_{\mu\nu} = 8\pi G T_{\mu\nu}. \tag{1.9}$$

Notice how the term $8\pi G\Lambda g_{\mu\nu}$ can either be understood as a geometrical term, thus appearing in the left hand side of the equation, or as another component in matter and energy with $w = -1$, and would then appear in the right hand side of the equation. The static and flat solutions with cold matter and cosmological constant require that $\rho_M = 2\rho_\Lambda$, where $\rho_\Lambda = \Lambda$, which can be shown to be an unstable solution [6] and suffers from fine tuning problems. Equation (1.9) can be derived from the action

$$S = \int d^4x \sqrt{-g} \left[\frac{1}{16\pi G} R - \Lambda \right] + S_m. \tag{1.10}$$

Although the search for a static solution was abandoned with the discovery of the expansion of the universe, the case of flat space dominated by a positive cosmological constant, known as De Sitter space, is still relevant. The Friedmann equation can be directly integrated to give

$$a(t) = e^{t/R_0}, \tag{1.11}$$

where $R_0 = \sqrt{\frac{3}{8\pi G\Lambda}}$ is De Sitter's radius. We have thus found a solution with accelerated expansion.

In general, it is possible to consider a flat universe dominated by a fluid with a general equation of state w. Energy conservation gives

$$\rho(t) = \rho_0 \left(\frac{a(t)}{a_0} \right)^{-3(w+1)}, \tag{1.12}$$

which hints the interpretation of the cosmological constant as a perfect fluid with constant density over time. Equation (1.7) states that in order to find accelerated expansion, it must hold that $w < -\frac{1}{3}$.

The first evidence for the accelerated expansion of the universe was found by High Z Supernovae Team and Supernova Cosmology Project ([23], [24]), coming from the observation of the magnitude of Type Ia supernovae at high redshifts z. Both teams found that the best fit for the luminosity distance at high z favour a positive cosmological constant Λ, and thus $\Omega_\Lambda > 0$.

1.1.3 ΛCDM model

With these ingredients, a general universe with cold dark matter, baryonic matter, radiation and a dark energy component with equation of state w will be governed by the Friedmann equation

$$H = \frac{\dot{a}}{a} = H_0 \sqrt{(\Omega_c + \Omega_b)a^{-3} + \Omega_{rad}a^{-4} + \Omega_k a^{-2} + \Omega_\Lambda a^{-3(1+w)}}, \tag{1.13}$$

where H is the Hubble parameter. The best fit for the density parameters can be obtained from observations, and for the dark energy component they point towards a perfect fluid with an energy density of

$$\rho_\Lambda \sim 10^{-47}\ \text{GeV}^4 \tag{1.14}$$

and a equation of state with parameter

$$w_\Lambda = -1.03 \pm 0.03, \tag{1.15}$$

compatible with a cosmological constant with $w = -1$ [1]. The density parameter for this component is

$$\Omega_\Lambda = 0.6847 \pm 0.0073. \tag{1.16}$$

This implies that in the present, the majority of the energy content of the universe is given by dark energy.

1.1.4 The cosmological constant problem

The theoretical value of the cosmological constant receives quantum corrections with quantities whose value is typically several orders of magnitude bigger than the measured one [20]. This mismatch can be explained tuning the classical contribution so it cancels the quantum corrections. However, this solution does not seem to be natural, thus giving rise to the cosmological constant problem.

1.2 Physics beyond ΛCDM

1.2.1 Dynamical dark energy

Now, we will study the possibility that the accelerated expansion of the universe arises from the potential energy of a field, and thus we will set $\Lambda = 0$. This mechanism can be particularly attractive, as it is similar to the one that explains cosmic inflation at early times, and presents the easiest extension of ΛCDM. The action that describes a scalar field minimally coupled to gravity is

$$S = \int d^4x \, \sqrt{-g} \left\{ \frac{M_{Pl}^2 R}{2} - \frac{1}{2}(\partial\phi)^2 - V(\phi) \right\}. \tag{1.17}$$

Its energy momentum tensor is given by

$$T_{\mu\nu} = \frac{2}{\sqrt{-g}} \frac{\delta(\sqrt{-g}\mathcal{L})}{\delta g^{\mu\nu}} = \partial_\mu\phi\partial_\nu\phi - g_{\mu\nu}\left(\frac{1}{2}(\partial\phi)^2 + V(\phi)\right). \tag{1.18}$$

Particularising this result for an homogeneous and isotropic spacetime, and comparing it to that of a perfect fluid, the pressure and the density of the field will be given by

$$\rho_\phi = \frac{1}{2}\dot{\phi}^2 + V(\phi) + \frac{1}{2}(\nabla\phi)^2, \tag{1.19}$$

$$P_\phi = \frac{1}{2}\dot{\phi}^2 - V(\phi) - \frac{1}{6}(\nabla\phi)^2. \tag{1.20}$$

In order for the field to cause late time acceleration, its effective mass must be of the order of the Hubble parameter, so its Compton wavelength will be of the order of

the Hubble scale. This argument leads us to consider the field spatially smooth inside the Hubble scale, and we can thus neglect the terms $\nabla\phi$ [19]. It is possible to insert the results for ρ_ϕ and P_ϕ in equations (1.6) and (1.7) to find the evolution of the scale factor a and the hubble parameter H. In order to reproduce the observed expansion, it must hold that

$$w_\phi = \frac{P}{\rho} = \frac{\frac{1}{2}\dot{\phi}^2 - V(\phi)}{\frac{1}{2}\dot{\phi}^2 + V(\phi)} \approx -1, \tag{1.21}$$

which requires that $\frac{1}{2}\dot{\phi}^2 \ll 1$, this is, the field rolls slowly towards its equilibrium value.

These models are usually referred to as *quintessence*, and they feature a large phenomenology of behaviours by choosing an appropriate potential $V(\phi)$. An interesting case is the Ratra-Peebles potential,

$$V(\phi) = \frac{M^{4+n}}{\phi^n}, \tag{1.22}$$

to which we will come back again in chapter 2. With this choice, the energy density of the field tracks the energy density of matter and radiation at early times, and only begins to dominate at later times [26]. The quintessence theories can be generalized to $K-$essence models, which will be further studied in chapter 3.

1.2.2 New degrees of freedom and fifth force

General Relativity is currently one of the best tested theories in modern physics. Moreover, it is the only theory for a Lorentz invariant massless particle with helicity 2 [11]. Thus, all new physics in the gravitational sector will involve introducing new degrees of freedom, which we will consider to be Lorentz scalars for simplicity.

If we impose that these scalars contribute to the vacuum energy, they must couple to the Standard Model fields at least via loops. Therefore, we expect that they mediate a force between these fields of range m_ϕ^{-1}. Assuming that the fields cancel the contribution of Λ up to an order of $\sim H_0^2 M_{\rm Pl}^2$, this mass should be smaller than the Hubble parameter, $m_\phi \lesssim H_0$, and so a fifth force will appear at cosmological distances and in the Solar System.

As a consequence, these theories make predictions that deviate from the ones from General Relativity in regions where it is extremely well tested. In the following sections, we will explore the ways by which we can go around this restriction, investigating how the force mediated by the scalar fields can hide through screening mechanism in dense regions such as our Solar System and escape the contraints from local tests.

1.3 Nature of screening mechanisms

We will now give an overview of the screening mechanisms that could hide the fields from our experiments, following the discussion found in [14].

1.3.1 Force-law classification

Let's derive the force associated with a given scalar field and investigate whether it naturally exhibits some kind of screening. We'll start with the general lagrangian given by

$$\mathcal{L} = -\frac{1}{2}Z^{\mu\nu}(\phi, \partial\phi, \ldots)\partial_\mu\phi\,\partial_\nu\phi - V(\phi) + g(\phi)T^{\mu}{}_{\mu}\,, \tag{1.23}$$

where $Z^{\mu\nu}$ represents the derivative self interactions of the field. At this point, we are making two assumptions regarding the coupling to matter, $g(\phi)$:

- **Universal coupling:** The coupling is the same for all matter, which is motivated by the universality of gravity. Some models of the chameleon mechanism do not make this assumption [15], which results in an explicit violation of the weak equivalence principle.
- **No derivative interactions with matter:** Such interactions would introduce other types of screening mechanisms [16], [21]. Also, those couplings would rise to forces that decay faster than $1/r^2$ so their effects on cosmological scales would be suppressed with respect to the usual gravitational force. While this is a possibility, we are interested in having cosmological effects while avoiding local gravity constraints.

The equations of motion for the field can be derived from Euler-Lagrange equations. In order to study the force mediated by this field, we will restrict our calculations to the classical regimen, assuming that the source is non relativistic (and thus $T^{\mu}_{\mu} \to -\rho$) and the space is flat. We can now work in the simplified configuration of a point source at the origin of mass M, $\rho = M\delta^3(\vec{r})$. For a given background configuration with a known solution $\bar{\phi}$, we can expand the field around it as $\phi = \bar{\phi} + \varphi$. To first order in φ, we find that

$$Z(\bar{\phi})\left(\ddot{\varphi} - c_s^2(\bar{\phi})\nabla^2\varphi\right) + m^2(\bar{\phi})\varphi = g(\bar{\phi})M\delta^3(\vec{r}). \tag{1.24}$$

In static conditions and neglecting the variations of $\bar{\phi}$ over the scale of our problem, we can describe the perturbation as governed by the effective potential

$$V(r) = -\frac{g^2(\bar{\phi})}{Z(\bar{\phi})e_s^2(\bar{\phi})}\frac{e^{-\frac{m(\bar{\phi})}{\sqrt{Z(\bar{\phi})}c_s(\bar{\phi})}r}}{4\pi r}M. \tag{1.25}$$

It is possible now to find solutions in which this field is screened near matter sources. For that, it should be noted that the parameters g, Z and m depend only on $\bar{\phi}$, which depends on the background. Thus, it is possible to define different screening mechanisms:

- **Weak coupling**: the coupling to matter $g(\bar{\phi})$ is very small in high density regions. This is the case of symmetron theories.
- **Large mass**: the mass fluctuations $m(\bar{\phi})$ are bigger in regions of high ambient density, so that the field effects are short range. Examples of this approach are chameleon theories.

- **Large intertia**: the function $Z(\bar{\phi})$ acquires a bigger value in high density regions. As mentioned previously, this term is related to the derivative self interactions of the field. In the case that the screening is activated when the second derivatives exceed a certain value, the mechanism is known as Vanshtein screening. If first derivatives are important, we are facing theories with kinetic screening, which will be further studied in chapter 3, where a computational approach to solve the static profile of these theories will be presented. It will be applied to Dirac-Born-Infeld (from now on, DBI) theory in chapter 4.

1.3.2 Phenomenological classification

In general, it is possible to consider another classification, based on the condition for the screening mechanisms to be activated:

- **Screening based on** ϕ: whether or not the scalar field ϕ is screened will depend on its value. These theories are subject to the action of a potential $V(\phi)$, and the screening mechanisms activate when the gravitational potential Φ exceeds the critical value of a certain energy scale Λ. It is the case of symmetron, chameleon or dilaton mechanisms.

- **Screening based on** $\partial\phi$: in this case, the screening mechanisms activate when the first derivatives of the field are bigger than a certain value, $\partial\phi \gtrsim \Lambda^2$. Examples of this mechanism are theories with kinetic self interactions know as $P(X)$, such as k-mouflage of DBI.

- **Screening based on** $\partial^2\phi$: lastly, we can find theories in which the screening mechanism turns on when the second derivatives of the field exceed a certain threshold: $\partial^2\phi \gtrsim \Lambda^3$. This is what we previously identified as Vanshtein screening, and can be found in theories such as Galileon [2] and massive gravity [3]. These are beyond the scope of this work.

1.4 Objectives of this work

The main objective of this work is to study screening mechanisms for scalar fields and to investigate the occurrence of regions where this screening becomes ineffective when dealing with systems containing more than one object. After providing a motivation for these theories and a brief classification of them, we will focus on the specific cases of the *symmetron* and *chameleon* fields. We will discuss their potential to induce self-acceleration of the universe and explore methods for obtaining numerical solutions for the field profiles of these scalar fields.

Then, we will turn our attention towards theories that exhibit kinetic screening mechanisms. In general, these are theories are governed by an equation that can only be solved in situations of high symmetry. We will obtain analytical results for simple scenarios and present approximated methods, which will be numerically checked. Additionally, we will develop a code based on the finite element method to determine the field profile in general situations, with a key feature of this code being its adaptability,

which allows for a finer mesh in regions of greatest interest and non-linearity. Finally, we will apply this to the Dirac-Born-Infeld model, validating the code by comparing it with analytical results. We will investigate the presence of descreened regions in two and three-body systems and assess the suitability of the approximation that we presented for these problems.

Chapter 2

Screening by deep potentials

Firstly, we will consider the theories in which the screening mechanisms are activated when ϕ exceeds a given value. In general, they will be governed by the action

$$S = \int d^4x \sqrt{-g} \left(\frac{M_{Pl}^2}{2} R - \frac{1}{2}(\partial\phi)^2 - V(\phi) \right) + S_{matter}[A^2(\phi) g_{\mu\nu}, \psi], \tag{2.1}$$

where $V(\phi)$ is a given potential that defines the theory and ψ are the matter fields. By appropriately choosing for the field $V(\phi)$ and the coupling to matter $A(\phi)$, it is possible to achieve a situation in which the force mediated by the scalar field is shut off in dense regions.

2.1 Equations of motion

We will now derive the equations of motion from (2.1). For the sake of simplicity, we will explicitly rewrite it as

$$S = \int d^4x \sqrt{-g} \left\{ \left(\frac{M_{Pl}^2}{2} R - \frac{1}{2}(\partial\phi)^2 - V(\phi) \right) + \frac{1}{\sqrt{-g}} \mathcal{L}_{matter}[A^2(\phi) g_{\mu\nu}, \psi] \right\}. \tag{2.2}$$

Defining the Jordan frame metric as $\tilde{g}_{\mu\nu} = A^2(\phi) g_{\mu\nu}$, the equations of motion can now be derived from Euler-Lagrange equations.

$$\frac{\partial \mathcal{L}}{\partial(\partial_\mu \phi)} = -\partial^\mu \phi \Rightarrow \partial_\mu \frac{\partial \mathcal{L}}{\partial(\partial_\mu \phi)} = -\partial_\mu \partial^\mu \phi = -\Box^2 \phi$$

$$\frac{\partial \mathcal{L}}{\partial \phi} = -V_{,\phi} + \frac{1}{\sqrt{-g}} \frac{\partial \mathcal{L}_{matter}}{\partial \phi}$$

$\mathcal{L}_{matter}$ depends on the field ϕ only through the Jordan frame metric. Thus,

$$\frac{\partial \mathcal{L}_{matter}}{\partial \phi} = 2A(\phi) A_{,\phi}(\phi) g_{\mu\nu} \frac{\partial \mathcal{L}_{matter}}{\partial \tilde{g}_{\mu\nu}} = \sqrt{-\tilde{g}} \tilde{T}^{\mu\nu} A(\phi) A_{,\phi}(\phi) g_{\mu\nu} =$$

$$= \sqrt{-g} \tilde{g}_{\mu\nu} \tilde{T}^{\mu\nu} A^3(\phi) A_{,\phi}(\phi) = \sqrt{-g} \tilde{T} A^3(\phi) A_{,\phi}(\phi),$$

where we used that $\sqrt{-g} = A^4(\phi)\sqrt{-g}$ and $\tilde{T}^{\mu\nu} = A^2(\phi) T^{\mu\nu}$, where $\tilde{T}^{\mu\nu}$ is the matter stress tensor in the Jordan frame. Gathering all the expressions, the equation of motion

for the field described by the action in equation (2.1) is

$$\Box^2\phi = V_{,\phi}(\phi) - A^3(\phi)A_{,\phi}\tilde{T}. \tag{2.3}$$

Defining the energy density as $\rho = A^{-1}(\phi)T_{matter} = A^3(\phi)\tilde{T}_{matter}$, this can be rewritten as a field subject to an effective potential as

$$\Box^2\phi = V_{\text{eff},\phi}(\phi), \text{ where } V_{\text{eff}}(\phi) = V(\phi) + A(\phi)\rho. \tag{2.4}$$

It is clear that the static profile and the dynamics of the field depend on our choice of the potential $V(\phi)$ and the coupling $A(\phi)$. We will now explore different possibilities that allow screening to appear.

2.2 Chameleon mechanism

The idea behind chameleon mechanism is that the field should acquire a large mass in dense regions, which results in the interaction having short range. This mass is defined as

$$m^2(\phi) = V^{\text{eff}}_{,\phi\phi}(\phi) = V_{,\phi\phi}(\phi) + A_{,\phi\phi}(\phi)\rho. \tag{2.5}$$

For static configurations, in order to find the profile of the field around a given mass distribution, we must solve the equation

$$\nabla^2\phi = V_{\text{eff},\phi}(\phi). \tag{2.6}$$

This equation is equivalent to that of a mass in a potential defined by $V_{\text{eff}}(\phi)$. Thus, we expect the background field to have values around its equilibrium point, where the derivative of the effective potential $V_{\text{eff},\phi}(\phi)$ vanishes. On the other hand, this family of theories is constrained by the fact that the variations in the chameleon field should be much smaller than Planck's mass. Consequently, we can express the coupling A via a series expansion as

$$A(\phi) \approx 1 + \xi\frac{\phi}{M_{Pl}}, \tag{2.7}$$

with ξ a constant parameter. If we impose that the force mediated by the chameleon field has gravitational strength in low density regions, ξ must be positive and of the order of unity. The same approximation can not be made for the potential $V(\phi)$, as it must contain a smaller mass scale in order to be able to produce a big range of field masses and eventually cosmological acceleration.

As an example of how this mechanism operates, we will use the Ratra-Peebles inverse power law potential, originally considered in [15]. It is given by

$$V(\phi) = \frac{M^{4+n}}{\phi^n}, \tag{2.8}$$

where n is a positive constant and M a mass scale. A graphical representation of the effective potential for different ambient densities is shown in figure 2.1, where the minimum for each value of ρ is explicitly marked. As we can see, the curvature in this minimum, related to the mass of the field fluctuations, is bigger for higher densities.

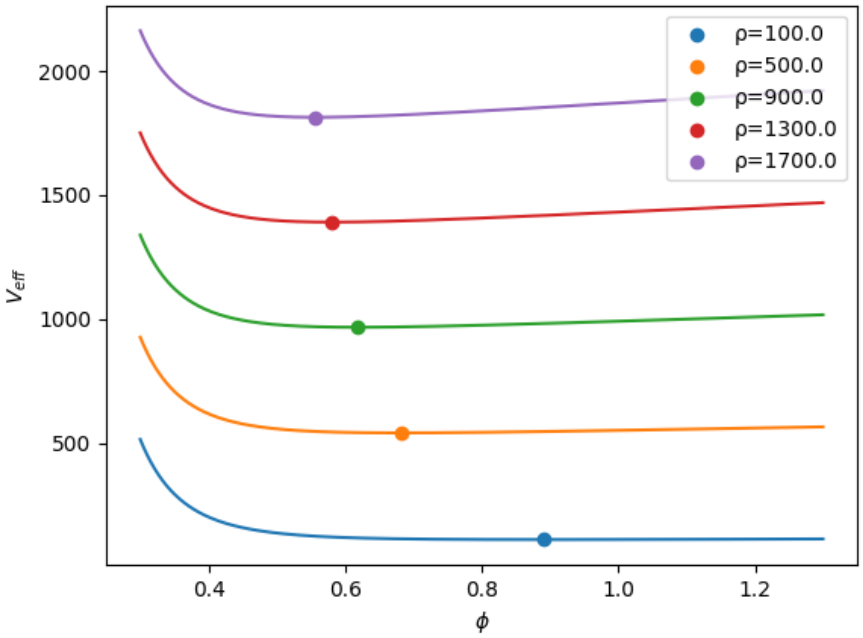

FIGURE 2.1: V_{eff} against ϕ for different densities. Dots mark the minimum value of the effective potential.

We will now calculate the mass of the field fluctuations for this potential, which is given by equation (2.5). In the equilibrium configuration, $\Box^2\phi = 0$, and we must therefore find the value of ϕ for which $V^{\text{eff}}(\phi)$ has a minimum:

$$\frac{\partial V^{\text{eff}}}{\partial \phi} = \frac{\xi\rho}{M_{Pl}} - \frac{nM^{4+n}}{\phi^{n+1}} = 0 \Rightarrow \phi_m(\rho) = \left(\frac{nM^{4+n}M_{Pl}}{\xi\rho}\right)^{\frac{1}{n+1}}. \tag{2.9}$$

We can now calculate the mass of the fluctuations as

$$m^2_{\text{eff}}(\phi) = \left(\frac{\partial^2 V_{eff}}{\partial\phi^2}\right)_{\phi_m} = \frac{n(n+1)M^{4+n}}{\phi_m^{n+2}} = n(n+1)M^{-\frac{n+4}{n+1}}\left(\frac{\xi\rho}{nM_{Pl}}\right)^{\frac{n+2}{n+1}}. \tag{2.10}$$

As expected, the mass of the fluctuations of the field is bigger in higher density regions, so the range of the interaction will be shorter.

2.2.1 Spherical solution

Lastly, we will study the field profile around a massive spherical object with density ρ_{obj} and radius R embedded in an ambient density ρ_{amb}. This ambient density could be

understood as the cosmological density if we where interested in the field profile near a cluster, or the average density of the Solar System if we were studying how the field behaves on Earth. Spherical symmetry allows us to rewrite equation (2.4) for a static field as

$$\frac{d^2\phi}{dr^2} + \frac{2}{r}\frac{d\phi}{dr} = \frac{dV(\phi)}{d\phi} + \xi\frac{\rho}{M_{Pl}}. \tag{2.11}$$

In order to solve this equation, it is natural to impose the following boundary conditions:

- $d\phi/dr$ vanishes at the origin.
- $\lim_{r\to\infty}\phi = \phi_{\text{amb}}$, where ϕ_{amb} is the value of the field given by equation (2.10) for $\rho = \rho_{\text{amb}}$.

We will suppose that the object is sufficiently large, so that the field approaches the minimum of its effective potential when $r < R$, with a small transition region that we will ignore in our first approximation. Outside of the object we expect the solution to have the form of Yukawa's potential. Thus, for distances such that $r < m_{\text{amb}}^{-1}$, we can approximate this solution as

$$\phi \approx \frac{A}{r} + B \text{ for } R < r < m_{\text{amb}}^{-1}. \tag{2.12}$$

We can match the boundary conditions as $\phi(R) = \phi_{\text{obj}}$ and $\phi(\infty) = B = \phi_{\text{amb}}$. Thus, the exterior solution can be expressed as

$$\phi(r) \approx -\frac{R}{r}(\phi_{\text{amb}} - \phi_{\text{obj}}) + \phi_{\text{amb}}. \tag{2.13}$$

The expression in equation (2.13) is only a first approximation to the solution of equation (2.11), but it allows us to further understand how the chameleon mechanism produces screening. For this, we shall calculate the derivative of our approximate solution that will give the force mediated by the field, which will be

$$\frac{d\phi}{dr} = \begin{cases} 0 & \text{if} \quad r < R \\ \\ \frac{R}{r^2}(\phi_{\text{amb}} - \phi_{\text{obj}}) & \text{if} \quad r > R \end{cases} \tag{2.14}$$

As we can see, a discontinuity in the derivative of the field of value $\frac{\phi_{\text{amb}} - \phi_{\text{obj}}}{R}$ appears at $r = R$. Given our previous considerations that the equation $\nabla^2\phi = 0$ holds at most of the space (which is a consequence of the fact that we suppose that the field approaches its equilibrium value), it is possible to establish a parallelism with classical electrostatics, in which discontinuities in the electric field (i.e. in the derivative of the scalar field) are caused by surface charges. In our case, we will consider that the *chameleon charge*, this is, the mass that couples to the chameleon field, is only to be found in a thin shell of radius ΔR. Considering that the mass in this thin shell can be

written as $\Delta M \approx 4\pi\rho R^2\Delta R$, by analogy with the result in electrostatics the value of this discontinuity can be written as

$$\left(\frac{d\phi}{dr}\right)_{R=R^+} - \left(\frac{d\phi}{dr}\right)_{R=R^-} = \frac{\xi\rho}{M_{Pl}}\Delta R. \tag{2.15}$$

Using the result from equation (2.14), it is possible to find the thickness of the shell, which will be given by

$$\frac{\Delta R}{R} = 4\pi M_{Pl} R\frac{\phi_{\text{amb}} - \phi_{\text{obj}}}{3\xi M}. \tag{2.16}$$

It is possible now to substitute the value found for $\phi_{\text{amb}} - \phi_{\text{obj}}$ in equation (2.13). Considering that the mass of the field is not negligible outside of the object, and writing again the Yukawa term, the exterior solution for the field is

$$\phi(r) = -\frac{3\xi}{4\pi M_{Pl}}\frac{\Delta R}{R}\frac{Me^{-m_{\text{amb}}(r-R)}}{r} + \phi_{\text{amb}} \text{ if } r > R. \tag{2.17}$$

It is clear that the result is the standard that we would get for a massive field, but with an additional term $\frac{\Delta R}{R} \ll 1$ that reduces the coupling. This is the case of a screened source. In this situation, gravity will couple to the whole mass of the object, and thus the field will be suppressed with respect to gravity. If the condition $\frac{\Delta R}{R} \ll 1$ does not hold, and thus $4\pi M_{Pl} R\frac{\phi_{\text{amb}}-\phi_{\text{obj}}}{3\xi M} \gtrsim 1$, it is said that the source is unscreened. The field will now couple to the whole mass of the object, and we recover the solution

$$\phi(r) = -\frac{\xi}{4\pi M_{Pl}}\frac{Me^{m_{\text{amb}}(r-R)}}{r} + \phi_{\text{amb}} \text{ if } r > R. \tag{2.18}$$

This happens when the mass of the object is small enough, and can be understood thinking that the field is not able to reach its equilibrium value inside the denser region.

2.3 Symmetron mechanism

A different choice of the coupling A and the potential $V(\phi)$ allows us to find situations in which the coupling to matter weakens in dense regions. In particular, we will consider that $A(\phi)$ is proportional to the vacuum expectation value of the field. Thus, $V(\phi)$ will be chosen so this value is zero in dense regions and nonzero in those of lower density. In particular, we will work with

$$A(\phi) = 1 + \frac{1}{2M^2}\phi^2, \tag{2.19}$$

where M is a mass scale, and

$$V(\phi) = -\frac{\mu^2}{2}\phi^2 + \frac{\lambda}{4}\phi^4. \tag{2.20}$$

As stated in equation (2.4), this setup can be identified with the effective potential

$$V_{\text{eff}}(\phi) = \frac{1}{2}\left(\frac{\rho}{M^2} - \mu^2\right)\phi^2 + \frac{\lambda}{4}\phi^4. \tag{2.21}$$

It is clear now that the effective potential depends on the ambient region ρ, and thus the behaviour of the field will also depend on it. This can be easily understood in figure 2.2: for high densities, $\frac{\rho}{M^2} - \mu^2 > 0$ and therefore the vacuum expected value will be zero, while for lower densities there is a broken symmetry and there will be two nonzero vacuum expected values.

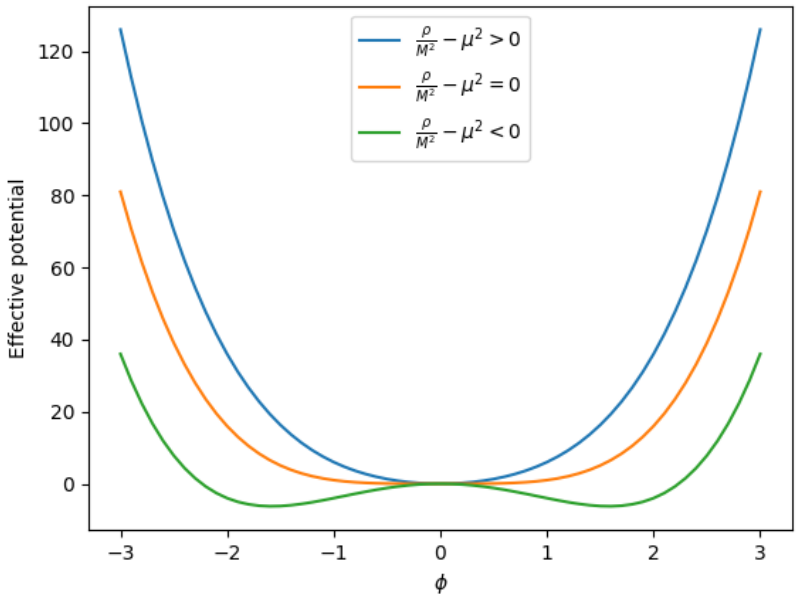

FIGURE 2.2: $V_{\text{eff}}(\phi)$ against ϕ for different values of the local density ρ.

After this qualitative approach, we will now move on to a more analytical study. The relative extremes of the effective potential will be given by

$$\frac{\partial V_{\text{eff}}}{\partial \phi} = \left(\frac{\rho}{M^2} - \mu^2\right)\phi + \lambda\phi^3 = 0 \Rightarrow \phi_0 = 0, \quad \phi_\pm = \pm\sqrt{\frac{\mu^2 - \frac{\rho}{M}}{\lambda}}. \tag{2.22}$$

The solution ϕ_0 will always exist, whereas $\phi_\pm$ will only exist when $\rho \leq \mu^2 M^2 \equiv \rho_{\text{break}}$. We can now check the stability of these points where the first derivative vanishes:

$$\frac{\partial^2 V_{\text{eff}}}{\partial \phi^2} = \left(\frac{\rho}{M^2} - \mu^2\right) + 3\lambda\phi^2 = \begin{cases} \left(\frac{\rho}{M^2} - \mu^2\right) & \phi = \phi_0 \\ -2\left(\frac{\rho}{M^2} - \mu^2\right) & \phi = \phi_{+,-} \end{cases} \tag{2.23}$$

Gathering the information from equations (2.22) and (2.23) it is possible to distinguish three different regimes:

- $\rho < \rho_{\text{break}}$: $\phi_0 = 0$ is a maximum and $\phi_\pm = \pm\sqrt{\frac{\mu^2 - \frac{\rho}{M}}{\lambda}}$ are minima.
- $\rho > \rho_{\text{break}}$: the only extreme is $\phi_0 = 0$ and it is a minimum.
- $\rho = \rho_{\text{break}}$: the only extreme is $\phi_0 = 0$ and it is an inflection point.

2.3.1 Spherical solution

Now that we have an understanding of the behaviour of the symmetron field in the presence of mass, it is the moment to try and find an analytical solution for a simple configuration. We will consider an object of density $\rho > \rho_{\text{break}}$ and radius R. Spherical symmetry allows us to rewrite equation (4.23) as

$$\frac{d^2\phi}{dr^2} + \frac{2}{r}\frac{d\phi}{dr} = \left(\frac{\rho}{M^2} - \mu^2\right)\phi + \lambda\phi^3. \tag{2.24}$$

Inside the source, we can consider that the value of the field will not be very far from its minimum value ϕ_0. Thus, it will be enough to consider the second order approximation of the effective potential:

$$V_{\text{eff}} \approx \left(\frac{\rho}{M^2} - \mu^2\right)\frac{\phi^2}{2}. \tag{2.25}$$

Equation (2.24) can be rewritten as

$$\frac{d^2\phi}{dr^2} + \frac{2}{r}\frac{d\phi}{dr} = \frac{1}{2}\left(\frac{\rho}{M^2} - \mu^2\right)\phi^2, \tag{2.26}$$

which can be easily solved with the change of variables $\phi = \frac{u}{r}$. Imposing that $\lim_{r\to 0}\frac{d\phi}{dr} = 0$, the solution for the field inside the source is

$$\phi_{\text{in}} \approx A\frac{R}{r}\sinh\left(r\sqrt{\frac{\rho}{M^2} - \mu^2}\right) \tag{2.27}$$

Outside the object it is possible to follow a similar approach. Approximating the effective potential around the equilibrium value $\phi_\pm$ and with the change of variables $\phi - \phi_\pm = \frac{u}{r}$, equation (2.24) gives

$$\frac{1}{r}\frac{d^2u}{dr^2} = \mu u. \tag{2.28}$$

The solutions to this equation are two real exponential functions. Far enough from the source, we expect to recover the solution from the background. Therefore, $\lim_{r\to\infty}\phi = \phi_\pm$, and the solution for the field outside the source is

$$\phi_{\text{out}} \approx B\frac{R}{r}e^{-\sqrt{2}\mu r} + \phi_\pm. \tag{2.29}$$

Notice how there is no distinction made between the cases when the equilibrium value reached by the field is ϕ_+ or $\phi_- = -\phi_+$, which is a consequence of the fact that the field always enters the equations squared and of the symmetry of the theory.

To find the values for the constants A and B, we must impose that solution is continuous and derivable. Following the calculations from [12], we will also define the parameter α, which measures the ratio between the Newtonian potential at the surface of the object and M/M_{Pl}:

$$\alpha = 6\frac{M_{\text{Pl}}^2}{M^2}\Phi = \frac{\rho R^2}{M^2}. \tag{2.30}$$

It is now possible to distinguish two situations:

- **Small object:** $\alpha \ll 1$. The constants will have the value

$$A = \phi_\pm \frac{1}{\sqrt{\alpha}}\left(1 - \frac{\alpha}{2}\right) \quad \text{and} \quad B = \phi_\pm \frac{\alpha}{3}. \tag{2.31}$$

- **Big object:** $\alpha \gg 1$. The constants will have the value

$$A = \phi_\pm \frac{2}{\sqrt{\alpha}} e^{-\sqrt{\alpha}} \quad \text{and} \quad B = \phi_\pm \left(-1 + \frac{1}{\sqrt{\alpha}}\right). \tag{2.32}$$

When comparing this analytical solution to the one that we will obtain numerically in the following section, we should expect that they approach similar values inside of the object and for $r \to \infty$, but they will differ in between, as a consequence of the second order approximation of the effective potential.

2.4 Numerical study

After this approximated analytical study, we carry on a numerical study. We will focus in solving the equation

$$\nabla^2 \phi = \frac{\partial V_{\text{eff}}(\phi)}{\partial \phi}, \tag{2.33}$$

where $V_{\text{eff}}(\phi)$ is given for each theory, and thus its derivative can be calculated. This equation can be seen as Poisson's equation with a source, which will also depend on the value of the field.

The procedure to numerically solve equation (2.33) is pretty straightforward through the finite differences method, as it can be easily discretized in a mesh, leading to an algebraic system of equations:

$$\begin{aligned} &\frac{u[i+1,j,k] + u[i-1,j,k] - 2u[i,j,k]}{h^2} + \frac{u[i,j+1,k] + u[i,j-1,k] - 2u[i,j,k]}{h^2} + \\ &+ \frac{u[i,j,k+1] + u[i,j,k-1] - 2u[i,j,k]}{h^2} = V_{\text{eff},\phi}(u[i,j,k]) \end{aligned} \tag{2.34}$$

In principle, equation (2.34) will be non linear in $u[i,j,k]$, which is our unknown, and can be written as $L[u] = 0$, where L is a certain operator. The approach will thus be

to use a modification of Gauss-Seidel's method that incorporates Newton-Raphson's iteration as done in [10]. For a guess $u_{\text{old}}[i,j,k]$ of the solution, a new guess will be given by

$$u_{\text{new}}[i,j,k] = u_{\text{old}}[i,j,k] - \frac{L[u_{\text{old}}[i,j,k]]}{\partial L[u_{\text{old}[i,j,k]}]/\partial u_{\text{old}}[i,j,k]}. \tag{2.35}$$

We will work with Dirichlet boundary conditions, imposing that the field reaches its equilibrium value in the edge of the mesh, which will only be true if the computational domain is sufficiently large. An implementation of this algorithm for the symmetron field with the potential and the coupling constant discussed above can be found in appendix A. For comparison, the analytical solution will be found following the method described above, and numerically calculating the coefficients A and B to ensure that the solution is continuous and differentiable.

The obtained numerical solution and the semianalytical solution can be found in figure 2.3. We see that, as expected, both solutions have a similar behaviour in those regions where their value is close to the equilibrium value, while there is a transition region outside of the source where they differ.

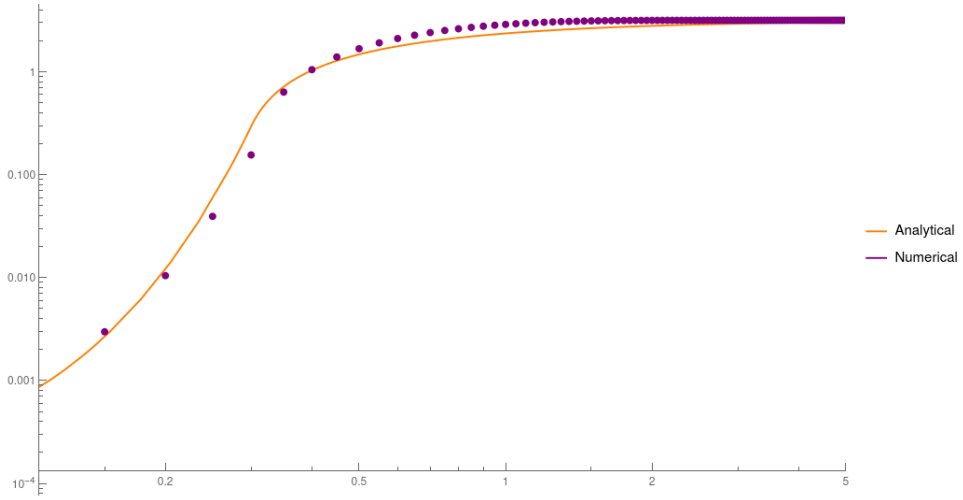

FIGURE 2.3: Numerical and semianalytical solutions for the symmetron field ϕ against r for a spherical source in the center of the mesh.

2.5 No-go result for self acceleration

We will now study the conditions under which this setup produces accelerated expansion of the universe in the absence of dark energy. As previously stated, we are working with the Jordan frame metric, $\tilde{g}_{\mu\nu}$, and the Einstein frame metric, $g_{\mu\nu}$, which are related through the conformal transformation

$$\tilde{g}_{\mu\nu} = A^2(\phi) g_{\mu\nu}. \tag{2.36}$$

The matter particles will couple to the Jordan frame metric, and it will be the one in which cosmological observations are made. On the other hand, it is in the Einstein

frame in which Friedmann equations take the standard form, and thus in which we shall require that $P < -\frac{1}{3}\rho$ in order to produce accelerated expansion.

Demanding that there is no dark energy, there should not be acceleration in the Einstein frame, and thus the accelerated expansion in the Jordan frame should arise from the conformal transformation (2.36). Therefore, $A(\phi)$ must change with time. In particular, relating the scale factors in both frames,

$$a_J = A\, a_E \Rightarrow (a\ddot{a})_J - (a\ddot{a})_E = \left(\frac{A'}{A}\right)', \tag{2.37}$$

where $'$ denotes derivative with respect to conformal time. If there is no dark energy in the Einstein frame, $(a\ddot{a})_E \leq 0$, and thus

$$(a\ddot{a})_J \leq \left(\frac{A'}{A}\right)'. \tag{2.38}$$

Over a Hubble time, this implies that

$$1 \lesssim \frac{\Delta A}{A}. \tag{2.39}$$

However, it can be shown that for chameleon-like theories, the requirement that the Milky Way galaxy is screened (and so local tests of gravity agree with theoretical results) implies that [25]

$$\frac{\Delta A}{A} \ll 1, \tag{2.40}$$

thus excluding the possibility of self-acceleration. It is still possible possible to obtain self-acceleration from the potential. In these cases, screening is still phenomenologically interesting, as it can give signals in the formation of structures.

Chapter 3

Kinetic screening

We will now discuss theories whose screening mechanisms are activated when the first derivative of the field exceeds a certain threshold. Each theory will be characterized by its kinetic term $K(X)$, where K is a certain function, and $X \equiv -\partial_\mu\varphi\partial^\mu\varphi$. They are defined by the action

$$S = \int d^4x \sqrt{-g}\left[\frac{M_{Pl}^2}{2}R + K(X)\right] + S_m(\Psi_i, \tilde{g}_{\mu\nu}), \tag{3.1}$$

where K is some funtion, $\tilde{g}_{\mu\nu} = A^2(\varphi)g_{\mu\nu}$ is the Jordan frame metric and Ψ_i are the matter fields. This family of theories appear naturally in various contexts, such as in some decoupling limits of spin-1 massive fields. Moreover, these theories are also interesting by themselves, as they allow for classical effects of irrelevant operators.

These theories have also been studied in relationship to the cosmological constant problem, as certain models $P(X, \varphi)$ can lead to self-acceleration of the expansion of the universe, as discussed in [4].

3.1 Equations of motion

Keeping the expansion to leading order in $\phi/M_{\rm Pl}$, the coupling to matter can be written as

$$A^2(\phi) \approx 1 + \frac{\alpha}{M_{\rm Pl}}\varphi. \tag{3.2}$$

In [18], higher order expansions have been considered, and the screening around a spherical object has been properly recovered. From the action (3.1), we can now find the equation of motion of the field [7], which is given by

$$\nabla_\mu(K_X\nabla^\mu\varphi) = -\frac{\alpha}{M_{\rm Pl}}T, \tag{3.3}$$

where $K_X = \frac{\partial K}{\partial X}$ and T is the trace of the matter stress-energy tensor.

In the static and non-relativistic limit, we can expand our expression at leading order in $1/c$. Until now, we have worked with units where $c = 1$. Restoring momentarily c, this yields

$$g_{\mu\nu} \approx \eta_{\mu\nu} + \mathcal{O}\left(\frac{1}{c^2}\right) \text{ and } \Box^2 \approx \nabla^2 + \mathcal{O}\left(\frac{1}{c^2}\right),$$

where $\eta_{\mu\nu}$ is the Minkowski metric for flat space. If the matter source is non relativistic, one can write $T = -\rho$. Thus, equation (3.3) gives

$$\nabla \left(K_X \nabla \varphi \right) = \frac{\alpha}{M_{\rm Pl}} \rho. \tag{3.4}$$

Our goal will be to solve equation (3.4) for different matter configurations, which can be identified as a non-lineal Poisson equation with a source. The non linearities arise from the term K_X and are a major difficulty when numerically solving for the static profile of the field.

3.1.1 Irrotational approximation

We will now solve equation (3.4) in the irrotational approximation, that will now be described. As a first approach, we shall define the vector

$$\vec{\mathcal{K}} = K_X \nabla \varphi. \tag{3.5}$$

Equation (3.4) can now be written as

$$\vec{\nabla} \cdot \vec{\mathcal{K}} = \frac{\alpha}{M_{\rm Pl}} \rho, \tag{3.6}$$

which greatly resembles Gauss law for electrostatics. Thus, it makes sense to use a decomposition analogous to the one that is typically used in electromagnetism. From Helmholtz's Theorem, we can write $\vec{\mathcal{K}}$ as

$$\vec{\mathcal{K}} = \nabla \psi + \vec{B}, \text{ where } \nabla \cdot \vec{B} = 0, \tag{3.7}$$

this is, $\vec{B}$ is the rotational of some field. Equation (3.6) thus gives

$$\nabla^2 \psi = \frac{\alpha}{M_{\rm Pl}} \rho, \tag{3.8}$$

whose solution for a point source is known from classical electromagnetism. It can also be solved for multiple or extense sources through linear superposition, giving

$$\psi(\mathbf{r}) = \frac{1}{4\pi M_{\rm Pl}} \int d^3\mathbf{r}' \frac{\alpha \rho(\mathbf{r}')}{\|\mathbf{r} - \mathbf{r}'\|}. \tag{3.9}$$

If the solenoidal component verifies that $\mathbf{B} = 0$, it is possible to square equation (3.5) to find

$$(\nabla \psi)^2 = K_X^2 \left(\nabla \varphi \right)^2 = -K_X^2 X, \tag{3.10}$$

which will be invertible if $K_X \neq 0$. Our problem would thus be solved, as we would have found an expression for X. However, whether the approximation $\mathbf{B} = 0$ is valid is not straightforward. In the following sections we will dig deeper into this question, comparing the irrotational approximated solution to the numerical results.

3.2 Polynomial $K-$essence

3.2.1 Point source

In order to understand how this screening mechanism operates, we will first consider the kinetic function

$$K(X) = X - \frac{1}{4}\frac{X^2}{\Lambda^4}, \tag{3.11}$$

where Λ is an energy scale. We shall work with a point mass at the origin, and thus $\rho = 4\pi m\delta^{(3)}(\mathbf{r})$. Equation (3.4) becomes

$$\nabla\left[\left(1 - \frac{X}{2\Lambda^4}\right)\nabla\phi\right] = \frac{\alpha}{M_{\rm Pl}} 4\pi m\delta^{(3)}(\mathbf{r}). \tag{3.12}$$

Integrating over the domain,

$$\left(1 - \frac{X}{2\Lambda^4}\right)\nabla\phi = \frac{\alpha}{M_{\rm Pl}}\frac{m}{r^2}\,. \tag{3.13}$$

This last expression can be simplified taking advantage of the spherical symmetry of the problem and using the definition for X. Thus,

$$\frac{\partial\varphi}{\partial r} + \frac{1}{2\Lambda^4}\left(\frac{\partial\varphi}{\partial r}\right)^3 = \frac{\alpha}{M_{\rm Pl}}\frac{m}{r^2}. \tag{3.14}$$

Defining the screening radius as

$$r_{\rm sc} = \frac{1}{\Lambda}\left(\frac{27}{8}\right)^{1/4}\sqrt{\frac{m\alpha}{4\pi M_{\rm Pl}}}, \tag{3.15}$$

the solution to equation (3.14) is

$$\varphi = -\frac{m}{4\pi r}\frac{\alpha}{M_{\rm Pl}}\,{}_3F_2\left[\frac{1}{4},\frac{1}{2},\frac{2}{3};\frac{5}{4},\frac{3}{2};-\left(\frac{r_{\rm sc}}{r}\right)^4\right], \tag{3.16}$$

where ${}_3F_2$ is the generalized hypergeometric function.

This expression does not give us much information, but it is useful two consider to regimes: close to the source and far from the source. For big radii, we expect that the derivative of the field is small, and thus the linear term in equation (3.14) will dominate. Following the same argument, close to the source it will be the cubic term the one that is not negligible. Thus, the derivative of the field will be

$$\frac{\partial\varphi}{\partial r} \approx \begin{cases} \frac{\alpha}{M_{\rm Pl}}\frac{m}{r^2} & r \gg r_{\rm sc} \\ \Lambda^{4/3}\left(\frac{2\alpha m}{M_{\rm Pl}}\right)^{1/3} r^{-2/3} & r \ll r_{\rm sc} \end{cases}. \tag{3.17}$$

The force mediated by a scalar field will be given by $\vec{F}_\varphi = \frac{\alpha}{M_{\rm Pl}}\nabla\varphi = \frac{\alpha}{M_{\rm Pl}}\frac{\partial\varphi}{\partial r}\hat{r}$. If we compare this result to the known expression for the gravitational force exerted by a point source, it is clear that the scalar field will mediate a force of the same strength as gravity far from the source provided $\alpha \sim 1$, but the ratio will be suppressed as $r^{4/3}$ inside the screening radius

3.2.2 Generalization

This mechanism can be generalized to kinetic screening theories that feature different expressions for $K(X)$. In particular, we could consider the general theory where

$$K(X) = \sum_{n=1}^{\infty} c_n \frac{X^n}{\Lambda^{4n-4}}. \tag{3.18}$$

It is clear that the scale $X/\Lambda^4 \sim 1$ will separate two different behaviours, and from now on we will identify it with the screening radius $r_{\rm sc}$. Far from the source, $X/\Lambda^4 \ll 1$, and thus $K(X) \approx c_1 X$. As a consequence, K_X will be a constant, and therefore equation (3.4) will be reduced to the usual Poisson's equation, showing the same behaviour as the gravitational field at large distances.

On the other hand, inside the screening radius $X/\Lambda^4 \gg 1$, and the higher order term will dominate. For a point source in the origin, equation (3.4) gives

$$K_X \nabla\phi = -\frac{\alpha}{M_{\rm Pl}}\frac{m}{r^2}. \tag{3.19}$$

If $c_n = 0$ for $n > N$, it will hold that $K(X) \approx c_N X^N/\Lambda^{4N-4}$, and as a consequence $K_X \approx N c_N X^{N-1}/\Lambda^{4N-4}$. Neglecting all the terms of lower order, this gives

$$A\left(\frac{\partial\varphi}{\partial r}\right)^{2N-1} = \frac{\alpha}{M_{\rm Pl}}\frac{m}{r^2}, \tag{3.20}$$

where A is some constant that groups all the parameters. Thus, $\left(\frac{\partial\varphi}{\partial r}\right) \sim r^{-\frac{2}{2N-1}}$, which gives us the dependence of the force mediated by the field near the source.

In particular, if the function $K(X)$ can be written as an infinite series, $N \to \infty$ and $\left(\frac{\partial\varphi}{\partial r}\right)$ is constant inside $r_{\rm sc}$. This is the case for Dirac-Born-Infeld theory, that is given by [9]

$$K_{\rm DBI} = \sqrt{1 + \frac{X}{\Lambda^4}}. \tag{3.21}$$

In chapter 4 we will explore in more detail the possibility of finding analytical solutions for the field profile in this theory, as well as some suitable approximations, and we will discuss them compared to numerical solutions.

3.3 Computational approach

We have seen that, even in the non-relativistic and static limit, the equations that need to be solved in order to understand the behaviour of the screening mechanisms are highly non linear. In particular, the static values of the field for a certain matter distribution can be calculated from

$$\nabla \left(K_X \nabla \varphi \right) = \frac{\alpha}{M_{Pl}} \rho, \tag{3.22}$$

where K_X is given by the theory. It is only possible to find analytical solutions in very symmetric conditions and for certain expressions for K_X. Thus, the existence of numerical solutions is essential in the study of these theories.

3.3.1 Finite element method

We will now describe the finite element method, which will be the basis of our approach. It will be applied to boundary value problems, in which Dirichlet boundary conditions for the value of the field in the borders will be specified. The implementation of this method will be done through the FEniCS library for Python [5].

The first step in the application of the finite element method is to discretize the computational domain into a set of convex elements, which can be arbitrary polyhedrons in 3D. A key feature of this method is that these elements do not need to have similar sizes, which allows us to create a coarser mesh in those regions where the solution does not change much, and to refine it near the regions where numerical difficulties are to be expected. This will be crucial for our problem, as we only expect the solution to change much around the screening scale. After this discretization, a family ψ_i of basis functions is defined. It is common that these are piece-wise polynomials, and their minimum order is that of the PDE being solved. For this problem, we will use Lagrange polynomials, which are already included in the functionalities of the FEniCS library.

The intended solution can be written in each element as a linear combination of these test functions:

$$\phi(x, y, z) = \sum_{i=1}^{N} a_i \psi_i(x, y, z), \tag{3.23}$$

where N is the number of elements. Notice how this expansion also allows us to calculate numerical derivatives as

$$\frac{\partial^n \phi(x, y, z)}{\partial x^n} = \sum_{i=1}^{N} a_i \frac{\partial^n \psi_i(x, y, z)}{\partial x^n}. \tag{3.24}$$

Our problem is now reduced to finding the undetermined coefficients a_i, which will yield to the solution to the posed equation.

3.3.2 Linear problem: weak form of partial differential equations

In the event that the partial differential equation to be solved is linear, we can now give a solution through an integral formulation. Let the equation be written as

$$A\phi = f, \tag{3.25}$$

where A is a linear operator, ϕ is the solution and f is some given function. The solution will be a function ϕ such that for all test functions v, the inner product of $A\phi$ and v equals the inner product of f and v, namely:

$$\langle A\phi, v\rangle = \langle f, v\rangle \ \ \forall v. \tag{3.26}$$

These test functions v are usually chosen so that they vanish on all boundaries where Dirichlet boundary conditions are defined.

We will choose the inner product of two functions f, g to be the integral of their product over all the computational domain

$$\langle f, g\rangle = \int_\Omega d^3x \ f(x,y,z)g(x,y,z), \tag{3.27}$$

although other choices are possible.

We will now make use of the linear decomposition of the solution ϕ and the test function v in the function basis:

$$\phi(x,y,z) = \sum_{i=1}^{N} a_i\psi_i(x,y,z),$$

$$v(x,y,z) = \sum_{i=1}^{N} b_i\psi_i(x,y,z).$$

Since A is, by definition, a linear operator, equation (3.26) must also hold for the functions of the basis. Thus,

$$\langle A\phi, \psi_i\rangle = \langle f, \psi_i\rangle \ \ i = 1, \dots, N. \tag{3.28}$$

Expanding the solution ϕ and using again the linearity of A,

$$A\phi = A\sum_{j=0}^{N} a_j\psi_j = \sum_{j=0}^{N} a_j(A\psi_j), \tag{3.29}$$

where $A\psi_j$ is a function that can be calculated, as both the operator A and the basis functions are known. Taking the inner product,

$$\langle A\phi, \psi_i\rangle = \int_\Omega d^3x \ \left(\sum_{j=0}^{N} a_j(A\psi_j)\right)\psi_j = \sum_{j=0}^{N} a_j \int_\Omega d^3x \ \psi_j A\psi_i = \sum_{j=0}^{N} \langle A\psi_j, \psi_i\rangle \, a_j. \tag{3.30}$$

Defining $f_i = \langle f, \psi_i \rangle$ and $m_{ij} = \langle A\psi_j, \psi_i \rangle$, equation (3.26) is now equivalent to

$$\sum_{i=1}^{N} m_{ij} a_j = f_i, \tag{3.31}$$

which can be rewritten in matrix form as

$$\boldsymbol{f} = \boldsymbol{M}\boldsymbol{a}. \tag{3.32}$$

We have now reduced our linear partial differential equation to a system of linear equations which can be solved using standard methods. This method is commonly used in the resolution of structural mechanics problems. As a consequence, the matrix $\boldsymbol{M}$ is often referred to as the stiffness matrix, and the vector $\boldsymbol{f}$ is usually known as the load vector.

3.3.3 Non linear problem: Newton's method

In the particular case of equation (3.22), the condition given by equation (3.26) can be written as

$$\int_\Omega d^3x \; v \, \nabla(K_X \nabla\phi) = \frac{\alpha}{M_{Pl}} \int_\Omega d^3x \; \rho \, v, \tag{3.33}$$

where v is the test function. Integrating by parts, it is posible to find a more symmetric formulation:

$$\int_\Omega d^3x \; v \, \nabla(K_X \nabla\phi) = -\int_\Omega d^3x \; \nabla v \cdot K_X \nabla\phi = \frac{\alpha}{M_{Pl}} \int_\Omega d^3x \; \rho \, v, \tag{3.34}$$

where the boundary terms vanish as a consequence of the definition of the test function v in the presence of Dirichlet boundary conditions. If we were working with Neumann boundary conditions, a term containing the derivatives in the boundaries should be added. However, it must be stressed that K_X is, in general, a non-linear function of the derivatives of the field, so our equation can not, in principle, be reduced to the simple linear form of (3.32).

The solution to this problem is to use Newton's method, an iterative method based on the supposition that we know an approximate solution $\phi^{(k)}$, and wish to find the true solution ϕ^*. Rewriting equation (3.34) as

$$F[\phi^*; v] = 0, \tag{3.35}$$

we can now expand the expression around the approximate solution $\phi^{(k)}$, using that $\phi^* = (\phi^* - \phi^{(k)}) + \phi^{(k)}$. Provided that $\phi^{(k)}$ and ϕ^* are sufficiently close, we can use functional derivation to linearize our problem as

$$0 = F[\phi^*; v] \approx F[\phi^{(k)}; v] + \int_\Omega d^3x \; \frac{\delta F}{\delta \phi}[\phi^{(k)}; v] \; (\phi^* - \phi^{(k)}), \tag{3.36}$$

which is a equation for $\delta\phi = \phi^* - \phi^{(k)}$ that must hold for any test function v and, in particular, for all the basis functions ψ_i.

The function $\phi^{(k+1)}$ for the next iteration is defined as

$$\phi^{(k+1)} = \phi^{(k)} + \delta\phi, \tag{3.37}$$

and the process continues until a certain tolerance is reached. The finite element method will be applied to each iteration of equation (3.36), thus yielding a linear system of equations to be solved.

This system of equations will be solved using the generalized residual method, which is an iterative procedure. For the system

$$Ax = b, \tag{3.38}$$

we will consider an initial guess x_0. The residual is given by

$$r_0 = b - Ax_0, \tag{3.39}$$

and we will define the vector v_1 as

$$v_1 = \frac{x_0}{|x_0|}. \tag{3.40}$$

For the $k-$th iteration, we will construct a basis $\{v_1, \ldots, v_k\}$ for the subspace $K_k(A, r_0) = \{r_0, Ar_0, \ldots, A^{k-1}r_0\}$. This can be done using the well knwonk Arnoldi's method. First, we can define

$$w = Av_k. \tag{3.41}$$

Thus, we can calculate h_{ij} as

$$h_{ij} = v_i^T w \text{ for } i = 1, \ldots, k. \tag{3.42}$$

It is now possible to define a new vector w' that is orthogonal to all the previous vectors of the basis as

$$w' = w - \sum_{i=1}^{k} h_{ij} v_i. \tag{3.43}$$

Now, $h_{k+1\,k} = |w'|$ and

$$v_{k+1} = \frac{w}{h_{k+1\,k}} \tag{3.44}$$

will be the new vector of the basis. The elements h_{ij} define a matrix H_k. Projecting the system $Ax = b$ in the subspace $K_k(A, r_0)$, the problem of minimising the residual is reduced to solving

$$\min\|(|r_0|(1, 0, \ldots 0) - H_k y)\|, \tag{3.45}$$

where $y \in K_k(A, r_0)$. The next iteration will be given by

$$x_k = x_0 + y^T V_k, \tag{3.46}$$

where $V_k = \{v_1, \ldots, v_k\}$, this is, y defines the coefficients for this linear combination.

This method is specially suitable for big matrices, as well as those that are not symmetric or positive definite. Thus, it will be interesting for our problem, as we will be looking into general configurations.

3.3.4 Accuracy control

One of the main features that make the finite element method attractive is the possibility of controlling with great detail the accuracy of our calculations. In particular, this can be improved by different means:

- **h-adaptativity**: A decrease in the size of the elements in which the computational domain is divided will, in general, lead to more accurate solutions. As stated previously, this subdivision does not need to be uniform throughout the domain, which allows us to perform less calculations in the regions in which the solution is smoother, and focus our work in those regions that can pose more problems from a numerical point of view.

- **p-adaptivity**: An increase in the degree of the basis functions leads again to an improvement of the accuracy. It must be noted that, in the case that the exact solution can be represented exactly with a polynomial of degree n, the numerical solution will be exact as long as we use basis functions of degree $n - 1$.

- **h-p adaptivity**: Conceived as an extension of the usual finite element method, this offers the possibility of using basis functions of different degrees in each element, which again allows to concentrate the more demanding calculations in the regions of interest.

Another advantage of the finite element method over other methods such as the finite differences method, which results in it being largely used for solving structural mechanics problems, is its ability to adapt to situations in which geometry is more complex by using a non uniform mesh.

3.3.5 Application to theories with kinetic screening

After this outline of the numerical method that will be used, we will now see how to apply it to problems of physical interest in order to solve equation (3.34) for a given K_X and a certain mater distribution. In particular, it will be interesting to take advantage of the h-adaptativity of the finite element method, making the mesh finer in the region where the screening mechanism is expected to operate. Since our work involves examining asymmetrical systems, we will refrain from employing any symmetrical reductions in the program that could be used to minimize computational expenses, as has been previously done in works such as [17] or [8]. Our aim will be instead to develop a code capable of solving the equations of the field under the most general circumstances as possible.

With this idea in mind, two codes will be written: one for a spherical mesh and another one for a square one. In both of them, Dirichlet boundary conditions will be

dictated, imposing that the field is constant in the edges. Thus, it will be necessary that these boundaries are far enough from the object, this is, that the mesh is sufficiently big. Additionally, we will refine the mesh around a certain radius r_{ref}, modifying the values of the radius r of the elements by the expression

$$r_{\text{mod}} = \frac{2}{\pi} r_{\text{ref}} \arctan(kr) \exp(ar^3 + br), \tag{3.47}$$

where k, a and b are positive constants. From now on, we will use that $k = 25$, $a = 5 \times 10^{-2}$ and $b = 3 \times 10^{-2}$ ([8]). The behaviour of this mesh modification can be easily understood in figure (3.1), that shows how the distance between two elements in the modified mesh is drastically decreased around r_{ref}, while it becomes very big far from this refinement radius. In general, we will chose the refinement radius r_{ref} to be the radius of the source, r_s.

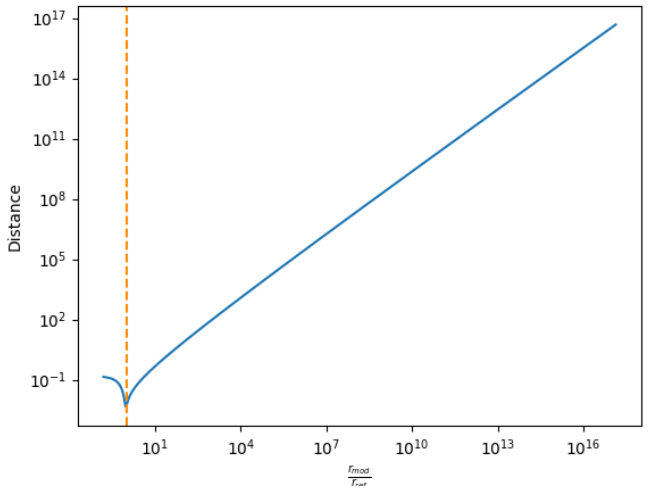

FIGURE 3.1: Distance between elements of the modified mesh against their distance to the origin. The distance is calculated as $r_{\text{mod},i+1} - r_{\text{mod},i}$, and the dashed line represents the refinement radius r_{ref}.

Chapter 4

Screening in Dirac-Born-Infeld theory

As mentioned earlier, the Dirac-Born-Infeld theory (from now on, DBI) is given by the kinetic function

$$K(X) = \sqrt{1 + \frac{X}{\Lambda^4}}. \tag{4.1}$$

We will start with a historical detour to motivate the choice for this $K(X)$, exploring the resemblance with nonlinear electrodynamics. After studying the analytical expressions and comparing with numerical results, we will finally study the breakdown of the screening mechanism in certain conditions, as well as the adequacy of the irrotational approximation that was previously introduced.

4.1 Born-Infeld model

The Born-Infeld model was introduced in 1934 to solve the divergence of the electron's self energy that appears in classical electrodynamics. The idea behind this model is to modify Maxwell's Lagrangian,

$$S = -\frac{1}{4}\int d^4\, \sqrt{-g} F_{\mu\nu}F^{\mu\nu}, \tag{4.2}$$

where $F_{\mu\nu} = \partial_\mu A_\nu - \partial_\nu A_\mu$, setting a maximum value for the electric field. This is done in a similar fashion as in the transition from the Newtonian action for a free particle to the relativistic one, in which the speed is limited by c.

Born first proposed the modified Maxwell Lagrangian to be

$$\mathcal{L} = b^2\left(\sqrt{1 - \frac{1}{2b^2}F_{\mu\nu}F^{\mu\nu}} - 1\right), \tag{4.3}$$

where b is the maximum value of the electric field. However, there is no other reason to choose this Lagrangian other than the requirement of finiteness of the electric field. After imposing that the theory is invariant under general coordinate transformations and that it recovers the known lagrangian for weak fields, the Born-Infeld action is given by

$$S_{BI} = -b^2\int d^4x\, \det\left(\sqrt{\eta_{\mu\nu} + \frac{1}{b}F_{\mu\nu}} - 1\right), \tag{4.4}$$

which can be rewritten as

$$S_{BI} = -b^2 \int d^4x \left(\sqrt{1 + \frac{1}{2b^2} F_{\mu\nu} F^{\mu\nu} - \frac{1}{16b^4} (F_{\mu\nu} \tilde{F}^{\mu\nu})^2} - 1 \right). \tag{4.5}$$

Substituting the definition of the electromagnetic tensor, it is possible to find that

$$S_{BI} = -b^2 \int d^4x \left(\sqrt{1 - \frac{\vec{E}^2 - \vec{B}^2}{b^2} - \frac{(\vec{E} \cdot \vec{B})^2}{b^4}} - 1 \right). \tag{4.6}$$

Equations (4.3) and (4.5) are equivalent for systems in which $\vec{B} = 0$. For a charge at rest, the lagrangian is thus given by

$$\mathcal{L}_{BI} = -b^2 \sqrt{1 - \frac{\vec{E}^2}{b^2}}. \tag{4.7}$$

Given that $\vec{E} = -\nabla\Phi$, where Φ is the electrostatic potential, it is clear now that equation (4.7) resembles the lagrangian given by the kinetic function (4.1) for static configurations. These same ideas can be applied to a scalar field, giving rise to DBI. This theory can also be obtained from theories with extra dimensions and string theories.

4.2 Isolated point mass

An interesting feature of DBI is that it allows to find an exact solution for simple situations. In particular, we will now consider the case for a point source of mass m. Thus, equation (3.4) becomes

$$\nabla \left(\frac{\nabla\varphi}{2\Lambda^4 \sqrt{1 + \frac{X}{\Lambda^4}}} \right) = \frac{\alpha}{M_{\rm Pl}} m \delta^{(3)}(\mathbf{r}). \tag{4.8}$$

Integrating once in the whole space yields

$$\frac{\nabla\varphi}{2\Lambda^4 \sqrt{1 + \frac{X}{\Lambda^4}}} = \frac{\alpha}{M_{4\pi \rm Pl}} \frac{m}{r^2}. \tag{4.9}$$

We can now make use of the spherical symmetry of our problem. As a consequence, $X = -\frac{1}{2}(\partial_r\varphi)^2$ and $\nabla\varphi = \partial_r\varphi$. Thus, equation (4.9) is reduced to

$$\frac{\partial_r\varphi}{2\Lambda^4 \sqrt{1 - \frac{(\partial_r\varphi)^2}{\Lambda^4}}} = \frac{\alpha}{4\pi M_{\rm Pl}} \frac{m}{r^2}, \tag{4.10}$$

which can be solved for $\partial_r\varphi$ to give

$$\frac{(\partial_r\varphi)^2}{\Lambda^4-(\partial_r\varphi)^2}=\frac{\alpha^2\Lambda^4}{4\pi^2M_{\rm Pl}^2}\frac{m^2}{r^4}\Rightarrow\partial_r\varphi=\frac{\Lambda^2}{\sqrt{1+\frac{M_{\rm Pl}^2}{4\alpha^2\Lambda^4m^2}r^4}}. \tag{4.11}$$

For the sake of simplicity, we can define the screening radius as $r_*^4=\frac{\alpha^2\Lambda^4m^2}{4\pi^2M_{\rm Pl}^2}$. Therefore,

$$\partial_r\varphi=\frac{\Lambda^2}{\sqrt{1+\left(\frac{r}{r_*}\right)^4}}. \tag{4.12}$$

Following this definition, the screening radius will be that at which the force mediated by φ is reduced to $1/\sqrt{2}$ its maximum value, and marks the scale at which the behaviour of $\partial_r\varphi$ changes.

Comparison with numerical result

The simplicity of the result in equation (4.12) is of great interest, as it allows for simple comparison with the numerical solution with the aim of validating the code. With this in mind, the setup for the code will be:

- Spherically symmetric mesh, refined around the theoretically calculated screening radius r_*.
- Dirichlet boundary conditions in the limits of the mesh, imposing that the field has a constant value over them.
- Spherical mass m of radius R located at the center of the mesh.

The use of these boundary conditions is explained by the spherical symmetry imposed by the source. On the other hand, the justification for using a finite mass will be further studied in section 4.4. For now, we will only be interested in the solution for the profile of the field outside of the source, and as it will be proved further on, this will be the same for both a finite source and a point one. The obtained result for $\partial_r\varphi$ is shown in figure 4.1, together with the analytical solution of (4.12), and as expected, the exterior profiles agree. The discrepancy at small r is a consequence of the resolution of the mesh.

4.3 Irrotational approximation

Following the discussion in section 3.1.1, it is possible to write the gradient of the field as

$$\frac{\nabla\varphi}{2\Lambda^4\sqrt{1+\frac{X}{\Lambda^4}}}=\nabla\psi+\vec{B}, \tag{4.13}$$

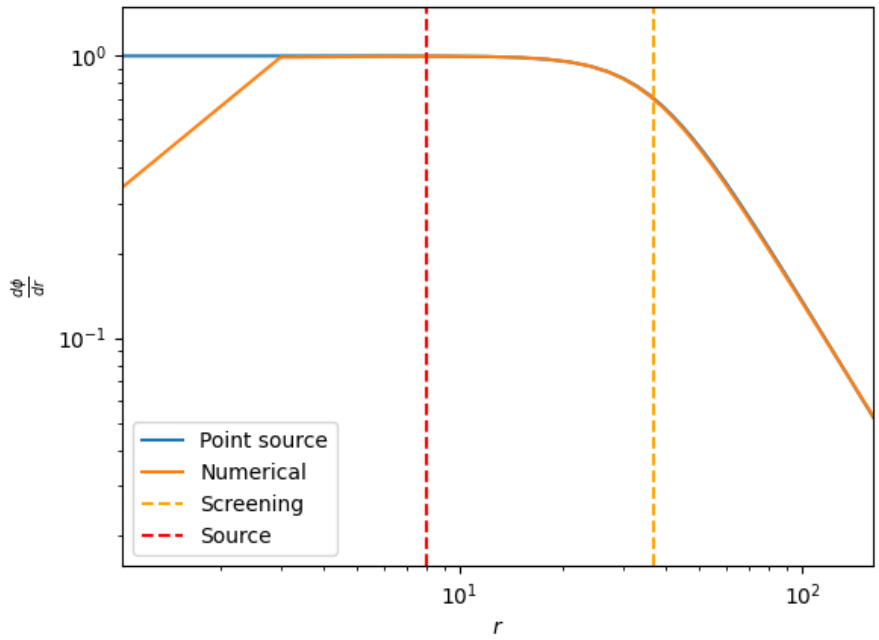

FIGURE 4.1: $\partial_r\varphi/\Lambda^2$ against r for a spherical mass at the origin. The blue line represents the analytical solution for a point mass. The dotted red line marks the radius of the spherical mass, while the dotted yellow line marks the screening radius r_*.

where $\nabla \cdot \vec{B} = 0$. Thus, equation (3.1) becomes

$$\nabla^2\psi = \frac{\alpha}{M_{Pl}}\rho, \tag{4.14}$$

which can be solved through linear superposition. For a system of n point masses located at positions $\vec{r}_i$, the solution is straightforward, and gives

$$\nabla\psi = \frac{\alpha}{4\pi M_{Pl}} \sum_i \frac{m_i}{|\vec{r} - \vec{r}_i|^3}(\vec{r} - \vec{r}_i) \tag{4.15}$$

As previously stated, the irrotational approximation involves considering that $\mathbf{B} = 0$, and thus

$$4\Lambda^4(\nabla\psi)^2 = -\frac{X}{\Lambda^4 + X} = \frac{(\nabla\varphi)^2}{\Lambda^4 - (\nabla\varphi)^2}. \tag{4.16}$$

This can be solved for $\nabla\varphi$, giving

$$\nabla\varphi = \frac{2\Lambda^2\nabla\psi}{\sqrt{1 + 4\frac{(\nabla\psi)^2}{\Lambda^4}}}, \tag{4.17}$$

where for a system of point masses $\nabla\psi$ will be given by equation (4.15).

An interesting case for the irrotational approximation is a system with spherical symmetry. In this case, the symmetry imposes that both $\nabla\psi$ and $\vec{B}$ are vectors that point in the radial direction. However, a radial vector with a vanishing divergence is necessarily the null vector, and thus $\vec{B} = 0$. Therefore, the irrotational approximation will be exact for spherically symmetric configurations.

4.4 Finite spherical mass

Using the result above, it is possible to generalise the solution for a point mass shown in equation (4.12) to a spherical mass m with a certain finite radius R located at the origin. The calculation of $\nabla\psi$ is analogous to the one found in classical electromagnetism, and it gives

$$\nabla\psi = \begin{cases} \frac{\alpha}{4\pi M_{Pl}} \frac{m}{r^2}\ \hat{u}_r & r > R \\ \\ \frac{\alpha}{4\pi M_{Pl}} \frac{m}{R^3} r\ \hat{u}_r & r < R \end{cases}. \tag{4.18}$$

Knowing that $\mathbf{B} = 0$ and taking into account that $\nabla\varphi$ is radial, the solution for the field outside of the source is given by

$$\partial_r\varphi = \frac{2\Lambda^2 \frac{\alpha}{4\pi M_{Pl}} \frac{m}{r^2}}{\sqrt{1 + 4\Lambda^4 \frac{\alpha^2}{16\pi^2 M_{Pl}^2} \frac{m^2}{r^4}}} = \frac{\Lambda^2}{\sqrt{1 + r^4 \frac{4\pi^2\Lambda^4 M_{Pl}^2}{\alpha^2 m^2}}}. \tag{4.19}$$

Recovering the definition of r_*^4, the exterior solution is identical to the one of a point mass, as expected. We can now work with the interior solution. Simple substitution gives

$$\partial_r\varphi = \frac{2\Lambda^2 \frac{\alpha}{4\pi M_{Pl}} \frac{m}{R^3} r}{\sqrt{1 + 4\Lambda^4 \frac{\alpha^2}{16\pi^2 M_{Pl}^2} \frac{m^2}{R^6} r^2}} = \frac{\Lambda^2 r}{\sqrt{r^2 + \frac{4\pi^2\Lambda^4 M_{Pl}^2 R^6}{\alpha^2 m^2}}} = \frac{\Lambda^2 r}{\sqrt{r^2 + \frac{R^6}{r_*^4}}}. \tag{4.20}$$

Thus, for a screened source mass (with $R < r_*$), the solution shows three different behaviours:

- $r >> r_*$: $\partial_r\varphi \sim r^{-2}$, identical to that of a point particle.
- $R < r < r_*$: $\partial_r\varphi$ saturates and is approximately constant.
- $r < R$: $\partial_r\varphi$ decreases as r approaches the origin, arriving to a nule value at $r = 0$.

4.5 Symmetries

In chapter 3, we discussed a theory with the kinetic function

$$K(X) = X - \frac{1}{4}\frac{X^2}{\Lambda^4}, \tag{4.21}$$

which can be seen as the first order expansion of equation (4.1). This can be seen the other way around, understanding DBI as a higher order extension of the previously

studied theories. The coefficients, however, are not arbitrary, and they are chosen so the action is invariant under certain symmetries. First, given that $X = -\partial_\mu\varphi\partial^\mu\varphi$ is a Lorentz scalar, it will be invariant under Lorentz transformations. It is also clear that S shows a shift symmetry,

$$\delta\varphi = c. \tag{4.22}$$

There exists a third more obscure symmetry, given by

$$\delta\varphi = v_\mu x^\mu - \varphi v_\mu\partial^\mu\varphi, \tag{4.23}$$

whose interpretation will be discussed further on.

We will now prove that the transformation given by equation (4.23) defines a symmetry of the DBI action:

$$\delta S = \int d^4x\ \sqrt{-g}K_X(X)\frac{\delta X}{\delta\varphi}\delta\varphi, \tag{4.24}$$

where δX can be calculated as

$$\frac{\delta X}{\delta\varphi} = -2\partial^\mu\varphi\partial_\mu\delta\varphi = -2v_\mu\partial^\mu\varphi - 2Xv^\mu\partial_\mu\varphi + 2\varphi v^\mu\partial^\alpha\varphi\partial_\mu\partial_\alpha\varphi. \tag{4.25}$$

The last term can be rewritten as

$$\varphi\partial^\alpha\varphi\partial_\mu\partial_\alpha\varphi = \partial_\mu(\varphi\partial^\alpha\varphi\partial_\alpha\varphi) + X\partial_\mu\varphi - \varphi\partial_\mu\partial^\alpha\varphi\partial_\alpha\varphi. \tag{4.26}$$

Thus,

$$\frac{\delta X}{\delta\varphi} = -2v_\mu\partial^\mu\varphi + 2v^\mu\partial_\alpha(\varphi\partial^\alpha\varphi\partial_\mu\varphi) - \varphi v^\mu(\partial_\mu\partial_\alpha\varphi\partial^\alpha\varphi), \tag{4.27}$$

and therefore δS will be given by

$$\delta S = \int d^4x\ \sqrt{-g}\ \partial_\mu(v^\mu\varphi\sqrt{1+X})\delta\varphi = \int d^4x\ \nabla_\mu(v^\mu\varphi\sqrt{1+X})\delta\varphi. \tag{4.28}$$

As the change in the Lagrangian is a total spacetime derivative, equation (4.23) defines a symmetry of this action.

An interesting way of understanding this symmetry comes from another interpretation of this theory: it arises from the action of a brane embedded in a flat 5-dimensional spacetime with two timelike dimensions [14]. Thus, the transformation (4.23) defines a 5-dimensional boost in a gauge in which $X^4 = \varphi$.

4.6 Descreened bubbles

We will now study whether there exist regions in which $\nabla\varphi$ has the same dependence as the classical Newtonian gravitational potential, and therefore there is a breakdown of the screening mechanism. When this happens, φ must verify Poisson's equation, which ψ also verifies, and thus $\nabla\varphi \propto \nabla\psi$. In the irrotational approximation, equation

(4.16) tells us that, for DBI,

$$X = -\frac{4(\nabla\psi)^2}{1+4\frac{(\nabla\psi)^2}{\Lambda^4}}, \tag{4.29}$$

where the term in the denominator is the responsible for the screening. Following the reasoning above, we will consider that the screening breaks down in a region in which $X \sim -4(\nabla\psi)^2$. For our system, this may happen when $\frac{(\nabla\psi)^2}{\Lambda^4} \lesssim 1$, this is,

$$|\nabla\psi| \lesssim \Lambda^2. \tag{4.30}$$

In general, when X is small enough, we expect that $K_X \sim$ constant, and thus equation (4.9) reduces to Poisson's equation.

4.6.1 Two body problem

As a consequence of these ideas, we will first study how the field behaves in the vicinity of the points where $\nabla\psi \sim 0$. With that objective, we shall consider a system with two equal point masses m, located at $z = \pm D/2$. In the irrotational approximation, it is possible to calculate the scalar field from

$$(\nabla\psi)_z = \frac{\alpha}{4\pi M_{\rm Pl}}\frac{m}{(z+D/2)^2} - \frac{\alpha}{4\pi M_{\rm Pl}}\frac{m}{(z-D/2)^2}, \tag{4.31}$$

and X can be calculated from equation (4.16). It is clear that in $z = 0$, $\nabla\psi = 0$. To first order around this point,

$$\nabla\psi = -\frac{8\alpha m}{\pi M_{\rm Pl}}\frac{1}{D^3}\left(z\hat{u}_z - \frac{1}{2}\rho\hat{u}_\rho\right). \tag{4.32}$$

Staying in the axis that joins both masses, and thus taking $\rho = 0$, the limits of this region where the screening breaks down and φ has the same spatial dependence as the gravitational field are given by

$$\frac{z_{\rm bubble}}{D} \sim \frac{\Lambda^2\pi M_{\rm Pl}D^2}{8\alpha m}. \tag{4.33}$$

This calculations can be easily generalized for a system of two bodies with different masses, defined as m and $q^{-1}m$ (with $q \geq 1$), located at $z = -D/2$ and $z = D/2$ respectively. The point where $\nabla\psi = 0$ is given by

$$z = \frac{D}{2}\frac{\sqrt{q}-1}{\sqrt{q}+1}, \tag{4.34}$$

and thus the size of the descreened region is [7]

$$\frac{z_{\rm bubble}}{D} \sim \frac{2\pi M_{\rm Pl}\Lambda^2 D^2}{m\alpha}\frac{q^{3/2}}{(1+\sqrt{q})^4}, \tag{4.35}$$

which reduces to the result in equation (4.33) in the case of $q = 1$ and two equal masses. This equation has an interesting consequence, as it suggests that, in the limit when one of these masses is much bigger than the other ($q \to \infty$), this unscreened region should disappear.

Although these results have been obtained in the irrotational approximation, it is clear that this effect will be observed in the full solution in those regions in which X is small. In particular, for $X \ll \Lambda^4$, $K_X \simeq (2\Lambda^4)^{-1}$, and thus the equation for φ is

$$\nabla^2\varphi \simeq 2\Lambda^4 \frac{\alpha}{M_{\rm Pl}}\rho. \tag{4.36}$$

We shall now study whether this region with a small X appears in the full numerical solution, and not only in the irrotational solution. In figure 4.2, we see that this unscreened region exists in a system with equal masses, even if the screened regions of the separated masses overlap. This result is relevant, as one might expect that a big mass with a screening radius large enough might screen all the smaller masses inside r_*, but we now know that there will appear regions in which X is small, and therefore $\nabla\varphi$ will be comparable with the newtonian potential.

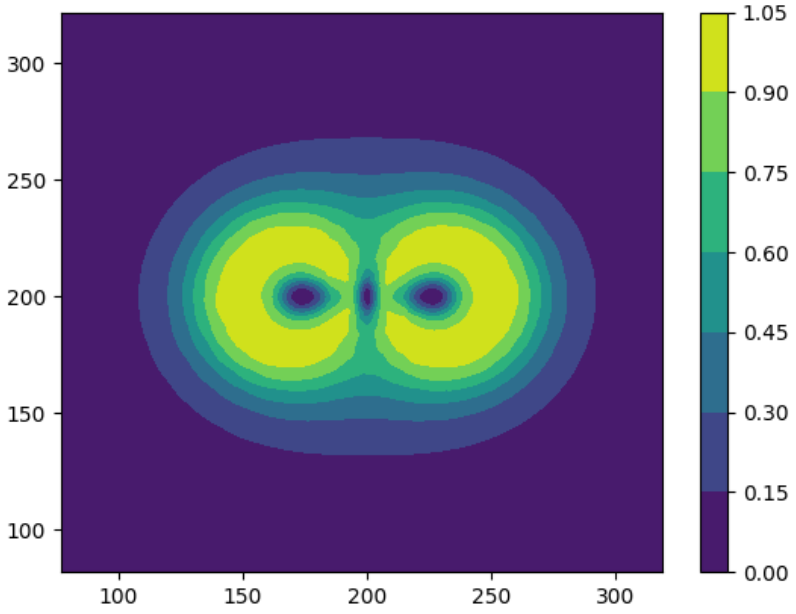

FIGURE 4.2: Contour plot of X/Λ^4 for a system of two equal masses. The distance between both masses is chosen so the screened regions overlap. We see that in this intersection, there appears an unscreened bubble.

The result obtained for two sources with different masses is shown in figure 4.3. As hinted by the results in the irrotational approximation, the unscreened region is now smaller.

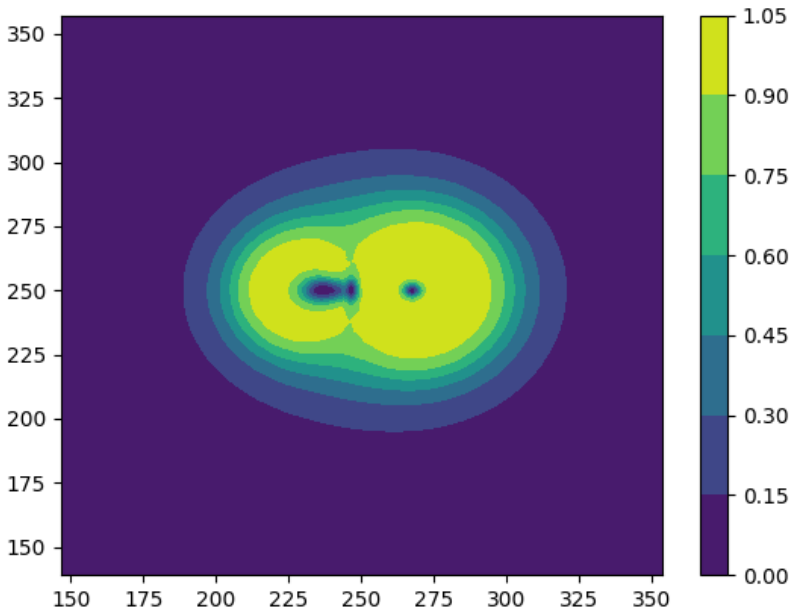

FIGURE 4.3: Contour plot of X/Λ^4 for a system of two sources verifying that $m_1 = 4m_2$.

For completeness, it is also interesting to check that, as implied by the reasoning above, $\nabla\varphi$ will have the same dependence as the Newtonian potential in those regions in which X is small. It particular, it will be enough to see that X has the same dependence as $4(\nabla\psi)^2$. This is shown in figure 4.4 for a system of two equal masses.

4.6.2 System of three bodies

The same approach can also be applied to more complex problems, such as systems of three bodies. The irrotational approximation suggests that we should also find descreened bubbles. Again, we can check this with the full numerical solution. The result for a system of three equal masses is shown in figure 4.5, and, as expected, we find a region in which the screening breaks down between the sources.

4.7 Validity of the irrotational approximation

As we have seen so far, it is clear that calculating the full solution to this problem can become very computationally demanding. Introducing the irrotational approximation can ease these difficulties, at the cost of reducing the precision of our solution. We will now study the validity of this approximation.

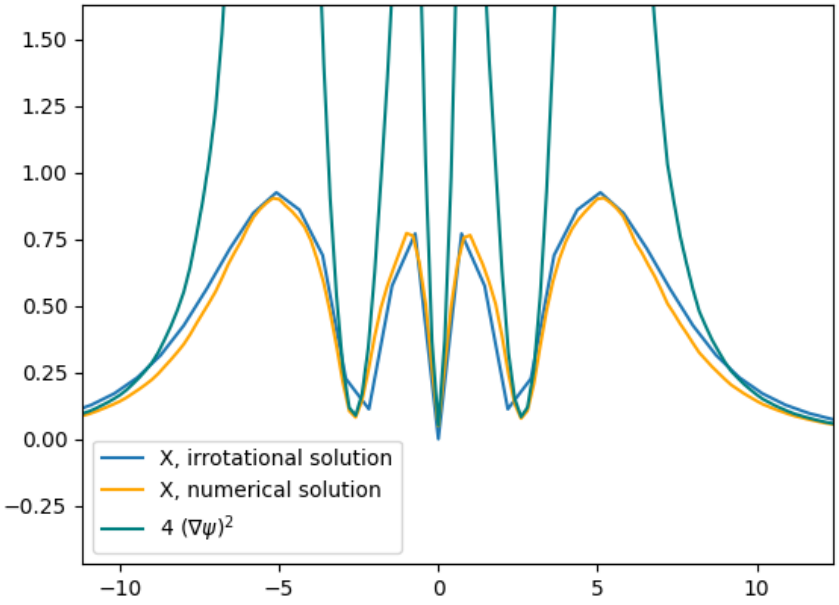

FIGURE 4.4: X calculated in the full numerical solution, together with the result from the irrotational approximation and $4(\nabla\psi)^2$.

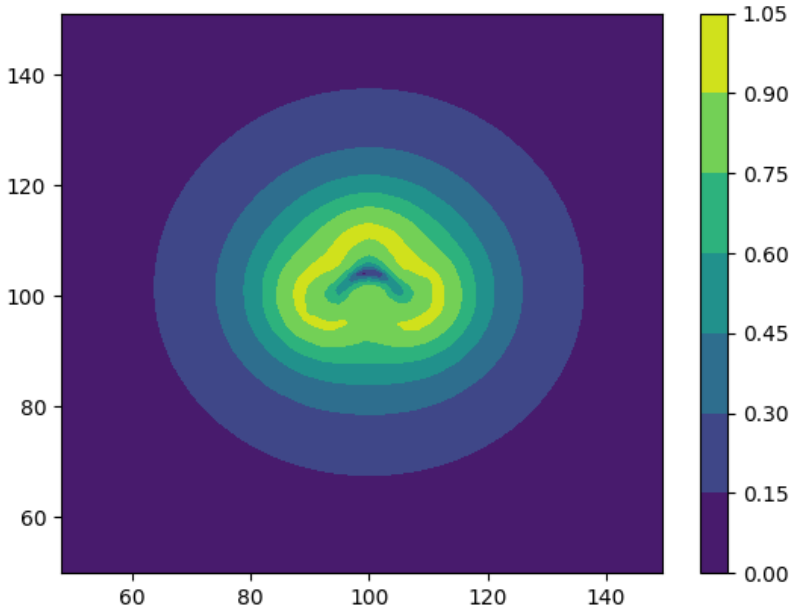

FIGURE 4.5: X/Λ^4 for a system of three equal masses in the plain that contains them.

Defining $\vec{E} = \nabla\varphi$, we are interested in solving

$$\nabla \cdot (K_X(\vec{E})\vec{E}) = \frac{\alpha}{M_{\rm Pl}}\rho. \tag{4.37}$$

The irrotational approximation is given by $\vec{E}_1 = \nabla\varphi_1$ such that also verifies equation (4.37). We know that it will be written as

$$K_X(\vec{E}_1)\vec{E}_1 = -\nabla\psi, \tag{4.38}$$

where

$$\nabla^2\psi = -\frac{\alpha}{M_{\rm Pl}}\rho. \tag{4.39}$$

On the other hand, the complete solution can be decomposed as

$$K_X(\vec{E})\vec{E} = -\nabla\psi + \mathbf{B}, \tag{4.40}$$

where ψ is the same as in the irrotational solution. As a first approximation, we will assume that $\vec{E}$ can be written as $\vec{E} = \vec{E}_1 + \vec{E}_2$, with $\vec{E}_2$ accounting for the rotational component. The irrotational approximation assumes that $|\vec{E}_1| \gg |\vec{E}_2|$. Therefore,

$$|\nabla\varphi|^2 \approx E_1^2 + 2\vec{E}_1 \cdot \vec{E}_2. \tag{4.41}$$

We will also consider that we are far enough from the sources, this is, that $|\vec{E}_1|^2 \ll \Lambda^4$. Staying at first order in $\vec{E}_1$,

$$K_X(\vec{E}_1 + \vec{E}_2)\vec{E}_1 = K_X(\vec{E}_1)\vec{E}_1 - \frac{\vec{E}_1 \cdot \vec{E}_2}{\Lambda^4}\frac{\vec{E}_1}{\sqrt{1 - \frac{E_1^2}{\Lambda^4}}} \tag{4.42}$$

and

$$K_X(\vec{E}_1 + \vec{E}_2)\vec{E}_2 = K_X(\vec{E}_1)\vec{E}_2 - \frac{\vec{E}_1 \cdot \vec{E}_2}{\Lambda^4}\frac{\vec{E}_2}{\sqrt{1 - \frac{E_1^2}{\Lambda^4}}}. \tag{4.43}$$

Taking into account that

$$K_X(\vec{E}_1 + \vec{E}_2)(\vec{E}_1 + \vec{E}_2) = K_X(\vec{E}_1)\vec{E}_1 + \mathbf{B}, \tag{4.44}$$

we find that

$$\mathbf{B} \approx K_X(\vec{E}_1)\vec{E}_2 - \frac{\vec{E}_1 \cdot \vec{E}_2}{\Lambda^4}\frac{(\vec{E}_1 + \vec{E}_2)}{\sqrt{1 - \frac{E_1^2}{\Lambda^4}}} = K_X(\vec{E}_1)\left(\vec{E}_2 - \frac{2\vec{E}_1 \cdot \vec{E}_2}{\Lambda^4}(\vec{E}_1 + \vec{E}_2)\right). \tag{4.45}$$

If the irrotational approximation is valid, we should be able to prove that $\mathbf{B}$ is small enough. In particular, to first order in $\vec{E}_1$ it holds that

$$\frac{\mathbf{B}}{|\vec{E}_2|} \sim 1 \Rightarrow \mathbf{B} \sim \vec{E}_2 \ll \vec{E}_1. \tag{4.46}$$

We see that the irrotational approximation is expected to be valid far from the sources, where $\vec{E}_1$ is small. However, it is not clear whether it gives good results in the proximity of the sources. This can be checked with the full numerical solution, comparing it with the solution obtained from the irrotational approximation. Specifically, we will do this for the two body problem. This is shown in figure 4.6 for the axis that joins both masses, and in figure 4.6 for the plain that contains them. As we can see, both results agree, giving very small differences. Thus, the irrotational approximation seems justified, as it gives similar results to the full solution even when $\nabla\varphi$ is big.

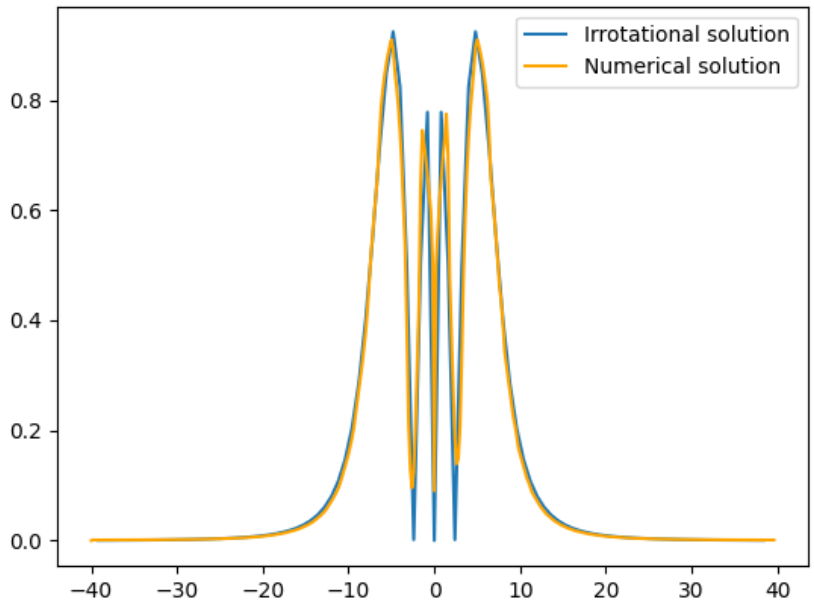

FIGURE 4.6: $\partial_r\varphi/\Lambda^2$ for a system with two equal masses in the axis that joins them. Both the numerical and the irrotational solution are shown.

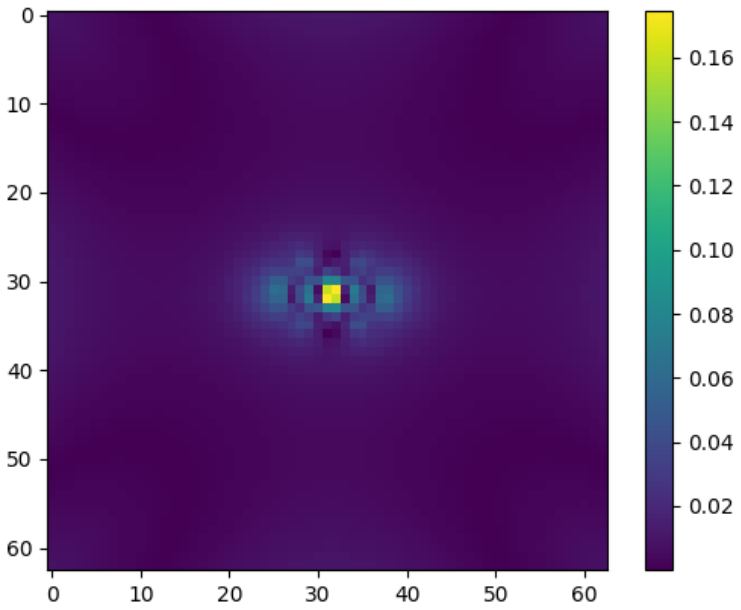

FIGURE 4.7: Difference between the values obtained for X/Λ^4 in the full numerical solution and in the irrotational approximation for a system of two equal masses in the plain that contains them.

Conclusions

In this work, we have studied the mechanisms through which theories that introduce new scalar fields in the gravitational sector allow the force mediated by these theories to be screened. After a review of these theories and obtaining some analytical and numerical results for both symmetron and chameleon mechanisms, we turned our attention to theories with kinetic screening.

Staying in the static and non-relativistic limit, we obtained the equation that defines the field profile for this setup, which can be seen as non-linear Poisson's equation. The complexity of this equation sparks the interest in the irrotational approximation, which simplifies the calculations through the principle of linear superposition. Then, we obtained a solution for a point source, and generalized this to theories that involve higher orders in the derivatives of the field. Lastly, we developed a code able to solve the profile of these fields for general configurations based on the finite element method, which we applied to the Dirac-Born-Infeld theory.

After obtaining analytical solutions for both point and spherical masses, we used these to validate the results of our code. With this in mind, we tackled the two body problem, and we proved the most interesting result in this work: the existence of regions between both masses in which the screening breaks down. We also checked that the irrotational approximation, which greatly reduces the computational cost of the obtainment of solutions, gives goods results for this theory. Lastly, we demonstrate that these descreened bubbles also appear in more complex problems, such as three body systems. This sets up interesting prospects for these theories, as the regions in which the screening breaks down offer the possibility of testing them. Additionally, we would expect that these regions have effects in the formation of cosmological structures.

Conclusiones

En este trabajo, hemos estudiado los mecanismos a través de los cuales las teorías que introducen nuevos campos escalares en el sector gravitacional permiten que la fuerza mediada por estas teorías sea apantallada. Después de una revisión de estas teorías y de obtener algunos resultados analíticos y numéricos para los mecanismos de *symmetron* y *chameleon*, centramos nuestra atención en las teorías con apantallamiento cinético.

Manteniéndonos en el límite estático y no relativista, obtuvimos la ecuación que define el perfil del campo para esta teoría, la cual puede verse como la ecuación de Poisson no lineal. La complejidad de esta ecuación motiva el interés en la aproximación irrotacional, que simplifica los cálculos a través del principio de superposición lineal. A continuación, obtuvimos una solución para una fuente puntual y la generalizamos a teorías que involucran órdenes superiores en las derivadas del campo.

Finalmente, desarrollamos un código capaz de resolver el perfil de estos campos para configuraciones generales basado en el método de elementos finitos, el cual aplicamos a la teoría de Dirac-Born-Infeld.

Tras obtener soluciones analíticas para masas puntuales y esféricas, utilizamos estas para validar los resultados de nuestro código. Con esto en mente, abordamos el problema de dos cuerpos, y probamos el resultado más interesante de este trabajo: la existencia de regiones entre ambas masas en las que el apantallamiento se rompe. También comprobamos que la aproximación irrotacional, que reduce considerablemente el coste computacional de la obtención de soluciones, da buenos resultados para esta teoría. Por último, demostramos que estas burbujas desapantalladas también aparecen en problemas más complejos, como sistemas de tres cuerpos. Esto abre perspectivas interesantes para estas teorías, ya que las regiones en las que se rompe el apantallamiento ofrecen la posibilidad de llevar a cabo tests. Además, cabría esperar que estas regiones tengan efectos en la formación de estructuras cosmológicas.

Appendix A

Codes

A.1 Screening by deep potentials

First, we present the code to find the profile of the field for a certain mass configuration in the *symmetron* and *chameleon* mechanisms. It is parallelized using the library MPI for Python.

```
import numpy as np
import matplotlib.pyplot as plt
from numpy import random
from mpi4py import MPI
import time
import math

comm = MPI.COMM_WORLD
rank = comm.Get_rank()
size = comm.Get_size()

m = 200
h = 0.01
T = 30
dt = 0.1
l = (m-1) * h # total length

M = 0.01
n = 4
Mp = 1 # This should be kept to 1, in order to work in units of the
       # Planck mass, which seems more natural
chi = 1
e = chi / Mp
mu = 0.0001
lam = 0.0001**2

# Assignation of initial values and scattering
if rank == 0:
    phis = np.zeros((m, m, m), dtype="double")
    us = np.zeros((m, m, m), dtype="double")
    phos = np.zeros((m, m, m), dtype="double")

    for i in np.arange(m):
        for j in np.arange(m):
            for k in np.arange(m):
                phis[i, j, k] = 1 + 0.2 * (random.rand() - 0.5)
```

```
                # !!! Weak field approximation

if rank == 0:
    ave, res = divmod(m, size)
    count = [ave + 1 if p < res else ave for p in range(size)]
    count = np.array(count)

    displ = [sum(count[:p]) for p in range(size)]
    displ = np.array(displ)
else:
    phis = None
    us = None
    phos = None
    count = np.zeros(size, dtype=int)
    displ = None

comm.Bcast(count, root=0)

# Initialization of the density field
if rank == 0:
    center = np.floor(m / 2)
    radius = np.floor(m / 50)
    for i in np.arange(m):
        for j in np.arange(m):
            for k in np.arange(m):
                dist2 = (i - m / 2)**2 + (j - m / 2)**2 + (k - m / 2)**2
                if dist2 < radius**2:
                    phos[i, j, k] = 200 * (1 - math.tanh(10 * dist2**0.5 -
                                radius * 10)) # Sharper distribution

if rank == 0:
    phi = np.array_split(phis, size)
    u = np.array_split(us, size)
    pho = np.array_split(phos, size)
else:
    phi = None
    u = None
    pho = None

if rank == 0:
    plt.figure()
    plt.imshow(phos[int(center), :, :], origin='lower', cmap='hot')
    plt.title('Initial conditions for the scalar field')
    plt.colorbar()
    print('Density field created')

phi = comm.scatter(phi, root=0)
u = comm.scatter(u, root=0)
pho = comm.scatter(pho, root=0)

def ghost(phi):
    # It also works with the matter density
    for r in range(size):
        if rank == r:
            d = phi.shape[0]
```

```
92              phi_ghost = np.zeros((d + 2, m, m), dtype="double")
93              phi_ghost[1:d + 1, :, :] = phi
94
95          if rank % size == (r - 1) % size:
96              comm.send(phi[-1, :, :], dest=r, tag=11)
97          elif rank % size == (r + 1) % size:
98              comm.send(phi[0, :, :], dest=r, tag=12)
99
100         if rank == r:
101             phi_ghost[0, :, :] = comm.recv(source=(r - 1) % size, tag=11)
102             phi_ghost[-1, :, :] = comm.recv(source=(r + 1) % size, tag=12)
103
104     return phi_ghost
105
106 def d1(phi, a):
107     if a == 0:
108         phig = ghost(phi)
109         d = (phig[2:, :, :] - phig[:-2, :, :]) / (2 * h)
110     else:
111         d = (np.roll(phi, -1, axis=a) - np.roll(phi, 1, axis=a)) / (2 * h)
112     return d
113
114 def laplace(phi):
115     phig = ghost(phi)
116     Lapl = (phig[2:, :, :] + phig[:-2, :, :] - 2 * phi) / h**2 + \
117         (np.roll(phi, +1, axis=1) + np.roll(phi, -1, axis=1) - 2 * phi) / h
                **2 + \
118         (np.roll(phi, +1, axis=2) + np.roll(phi, -1, axis=2) - 2 * phi) / h
                **2
119     return Lapl
120
121 """
122 #Functions related to chameleon screening
123 """
124 # IMPORTANT: WE ARE WORKING IN THE APPROXIMATION OF NON RELATIVISTIC
125 # MATTER UP TO FIRST ORDER (neglect post-newtonian terms in the
126 # stress-energy tensor)
127
128 # Function that solves the initial value using a relaxation method
129 def compute(phi, ni):
130     for i in np.arange(ni):
131         phig = ghost(phi)
132         phi = 1 / 6 * (phig[2:, :, :] + phig[:-2, :, :]  + \
133             np.roll(phi, 1, axis=1) + np.roll(phi, -1, axis=1) + \
134             np.roll(phi, 1, axis=2) + np.roll(phi, -1, axis=2) -
135             h**2 * dveff(phi, 4, pho))
136     return phi
137
138 def gauss_seidel(phi, ni):
139     for i in np.arange(ni):
140         phi_old = phi * 1.
141         L = laplace(phi) - dveff(phi, 4, pho)
142         dL = (- 2 * np.ones((count[rank], m, m), dtype="float")) / h**2 + \
143             (- 2 * np.ones((count[rank], m, m), dtype="float")) / h**2 + \
144             (- 2 * np.ones((count[rank], m, m), dtype="float")) / h**2 - \
```

```
            (pho / M**2 - mu**2) * np.ones((count[rank], m, m),
            dtype="float") - 3 * lam * phi**2

        phi = phi_old - np.divide(L, dL)
    return phi

# Function that defines the coupling of our field. It calculates the
# coupling for each value
def A_i(phi_i):
    a = 1 + chi / Mp * phi_i
    return a

# Derivative of the effective potential, used in the evolution of the
# field
def dveff(phi, n, pho):
    d = (pho / M**2 - mu**2) * phi + lam * phi**3
    return d

phi = gauss_seidel(phi, 300)

print('Evolution completed in rank {}'.format(rank))

recPhi = comm.gather(phi, root=0)

if rank == 0:
    recPhiv = np.concatenate(recPhi)
    print('The program has finished')
```

A.2 Kinetic screening

Bellow, it is shown the code written to numerically find the field profile for general configurations for theories with kinetic screening. In this case, a spherical mass at the origin is considered.

A.2.1 Square mesh

For the sake of simplicity, we first present the case in which a square mesh is constructed.

```
import numpy as np
from dolfin import *
import mshr
import matplotlib.pyplot as plt
from numpy.random import random
import math

# Sub domain for Dirichlet boundary condition. It is a boolean function
def boundary_boolean_function(x, on_boundary):
    return on_boundary

"""
```

```
PARAMETERS
"""

Lam = 1. # Energy scalre
mass = 3 # Density
rs = 8. # Radius of the source
mpl = 1. # Planck mass
G = 1. # Coupling constant

m_ = mass * 4./3. * np.pi * rs**3

rstar = 1/Lam * (G * m_/(4 * np.pi * mpl))**0.5 * np.sqrt(2.) # Screening
    radius

print("rs = {}".format(rs))
print("rstar = {}".format(rstar))

if rs > rstar:
    print("Object is not screened")
    exit()
else:
    print("rs < r screening. The object is screened.")
radio = 200

def symmetric_mesh3d(Nx, Ny, Nz, rstar):
    # Create a cubic mesh
    xmax = 4.5
    m = BoxMesh(Point(-xmax, -xmax, -xmax), Point(xmax, xmax, xmax),
                Nx, Ny, Nz)
    x = m.coordinates()
    # Modify the coordinates as desired
    for i in range(len(x)):
        if x[i, 0] != 0:
            x[i, 0] = rstar * (2/np.pi) * np.arctan(25 * abs(x[i, 0])) * \
                      np.exp(0.005 * abs(x[i, 0]) + 0.03 * abs(x[i, 0])**3)
                          * \
                      x[i,0]/abs(x[i,0])
        if x[i, 1] != 0:
            x[i, 1] = rstar * (2/np.pi) * np.arctan(25 * abs(x[i, 1])) * \
                      np.exp(0.005 * abs(x[i, 1]) + 0.03 * abs(x[i, 1])**3)
                          * \
                      x[i,1]/abs(x[i,1])
        if x[i, 2] != 0:
            x[i, 2] = rstar * (2/np.pi) * np.arctan(25 * abs(x[i, 2])) * \
                      np.exp(0.005 * abs(x[i, 2]) + 0.03 * abs(x[i, 2])**3)
                          * \
                      x[i,2]/abs(x[i,2])
    return m

mesh = symmetric_mesh3d(95, 95, 95, rs)

V = FunctionSpace(mesh, "CG", 2)

# Define boundary condition
g = Constant(1.) # Impose that the field has a constant value in the limits
```

```
bc = DirichletBC(V, g, boundary_boolean_function)

u = interpolate(Expression("sqrt(pow(x[0], 2) + pow(x[1], 2) + pow(x[2], 2)) / "
                           "sqrt(1 + (pow(x[0], 2) + pow(x[1], 2) + pow(x[2], 2))"
                           "/ pow(25, 2))", degree = 2), V)

v = TestFunction(V)

f = Expression("-3.*(sqrt(pow(x[0], 2) + pow(x[1], 2) + pow(x[2], 2)) < 8.)",
               degree=2) # Density
F = inner((1./sqrt(abs(1 - Lam**(-4)*inner(grad(u),grad(u))/2)))*grad(u),
          grad(v))*dx + f*v*dx

# Compute solution
M = u * dx
du = TrialFunction(V)
J = derivative(F, u, du) # Jacobian

solve(F == 0, u, bc, J=J,
    solver_parameters = {
    "newton_solver": {
        "linear_solver": "gmres",
        "preconditioner": "ilu",
        "relative_tolerance": 1.e-4,
        "absolute_tolerance": 3.e-4
    }
})
```

A.2.2 Spherical mesh

For situations with spherical symmetry, it will be useful to work with a spherical mesh, so that the boundary conditions respect the symmetry. The code will be identical, with the only difference being the definition of the mesh, that can be done as shown bellow.

```
radio = 4.6
num_meridianos = 20
num_paralelos = 20

geometry = mshr.Sphere(Point(0., 0., 0.), radio)
mesh = mshr.generate_mesh(geometry, num_meridianos)

"""plot(mesh, title='Spherical mesh')
plt.show()"""

def mesh3d(mesh, rstar):
    x = mesh.coordinates()

    for i in np.arange(len(x)):
        r = math.sqrt(x[i, 0]**2 + x[i, 1]**2 + x[i, 2]**2)
        theta = math.atan2(math.sqrt(x[i, 0]**2 + x[i, 1]**2), x[i, 2])
```

```
        phi = math.atan2(x[i, 1], x[i, 0])

        # Transform the radius
        r = rstar * (2/np.pi) * np.arctan(25 * r) * \
            np.exp(0.004 * r + 0.03 * r**3)
        # Calculate the new coordinates
        x[i, 0] = r * np.sin(theta) * np.cos(phi)
        x[i, 1] = r * np.sin(theta) * np.sin(phi)
        x[i, 2] = r * np.cos(theta)
    return mesh

mesh = mesh3d(mesh, rstar*2)
```

Bibliography

[1] N. Aghanim et al. “Planck2018 results: VI. Cosmological parameters”. *Astronomy amp; Astrophysics* 641 (Sept. 2020), A6.

[2] K. Aoki and K. Shimada. “Galileon and generalized Galileon with projective invariance in a metric-affine formalism”. *Physical Review D* 98.4 (Aug. 2018).

[3] N. Arkani-Hamed, H. Georgi, and M. D. Schwartz. “Effective field theory for massive gravitons and gravity in theory space”. *Annals of Physics* 305.2 (June 2003), 96–118.

[4] C. Armendariz-Picon, V. Mukhanov, and P. J. Steinhardt. “Dynamical Solution to the Problem of a Small Cosmological Constant and Late-Time Cosmic Acceleration”. *Physical Review Letters* 85.21 (Nov. 2000), 4438–4441.

[5] I. A. Baratta et al. “DOLFINx: The next generation FEniCS problem solving environment”. *preprint* (2023).

[6] W. B. Bonnor. “The instability of the Einstein universe”. *Monthly Notices of the Royal Astronomical Society* 115 (1955), p. 310.

[7] M. Bošković and E. Barausse. “Two-body problem in theories with kinetic screening”. *Physical Review D* 108.6 (Sept. 2023).

[8] J. Braden et al. “enics: Vainshtein screening with the finite element method”. *Journal of Cosmology and Astroparticle Physics* 2021.03 (Mar. 2021), p. 010.

[9] C. Burrage and J. Khoury. “Screening of scalar fields in Dirac-Born-Infeld theory”. *Physical Review D* 90.2 (July 2014).

[10] A.-C. Davis et al. “Structure Formation in the Symmetron Model”. *The Astrophysical Journal* 748.1 (Mar. 2012), p. 61.

[11] S. N. Gupta. “Quantization of Einstein’s Gravitational Field: General Treatment”. *Proceedings of the Physical Society. Section A* 65.8 (1952), p. 608.

[12] K. Hinterbichler and J. Khoury. “Screening Long-Range Forces through Local Symmetry Restoration”. *Physical Review Letters* 104.23 (June 2010).

[13] J. B. Jiménez, D. Bettoni, and P. Brax. “Polarisability and magnetisation of electrically K-mouflaged objects: the Born-Infeld ModMax case study” (2022).

[14] A. Joyce et al. “Beyond the cosmological standard model”. *Physics Reports* 568 (Mar. 2015), 1–98.

[15] J. Khoury and A. Weltman. “Chameleon cosmology”. *Physical Review D* 69.4 (Feb. 2004).

[16] T. S. Koivisto, D. F. Mota, and M. Zumalacárregui. "Screening Modifications of Gravity Through Disformally Coupled Fields". *Physical Review Letters* 109.24 (Dec. 2012).

[17] A. Kuntz, F. Serra, and E. Trincherini. "Effective two-body approach to the hierarchical three-body problem". *Phys. Rev. D* 104.2 (2021), p. 024016.

[18] G. Lara et al. "Robustness of kinetic screening against matter coupling". *Physical Review D* 107.4 (Feb. 2023).

[19] E. V. Linder. "The dynamics of quintessence, the quintessence of dynamics". *General Relativity and Gravitation* 40.2–3 (Dec. 2007), 329–356.

[20] J. Martin. "Everything you always wanted to know about the cosmological constant problem (but were afraid to ask)". *Comptes Rendus. Physique* 13.6–7 (July 2012), 566–665.

[21] J. Noller. "Derivative chameleons". *Journal of Cosmology and Astroparticle Physics* 2012.07 (July 2012), 013–013.

[22] S. R. Ovshinsky and H. Fritzsche. "Comment on "Vacuum catastrophe: An elementary exposition of the cosmological constant problem," by Ronald J. Adler, Brendan Casey, and Ovid C. Jacob". *American Journal of Physics* 65.9 (1997), p. 927.

[23] S. Perlmutter et al. "Measurements of and from 42 High-Redshift Supernovae". *The Astrophysical Journal* 517.2 (June 1999), 565–586.

[24] A. G. Riess et al. "Observational Evidence from Supernovae for an Accelerating Universe and a Cosmological Constant". *The Astronomical Journal* 116.3 (Sept. 1998), 1009–1038.

[25] J. Wang, L. Hui, and J. Khoury. "No-Go Theorems for Generalized Chameleon Field Theories". *Physical Review Letters* 109.24 (Dec. 2012).

[26] C. Wetterich. *The cosmon model for an asymptotically vanishing time-dependent cosmological "constant"*. 1994.